ADVANCED HEALTHCARE MATERIALS
www.advhealthmat.com

Enhancing the Accumulation of Polymer Micelles by Selectively Dilating Tumor Blood Vessels with NO for Highly Effective Cancer Treatment

*Guoqing Wei, Yi Wang, Xuehui Huang, Guang Yang, Jingya Zhao, and Shaobing Zhou**

The accumulation of nanoparticles in tumors by the enhanced permeability and retention (EPR) effect is effective and well known. However, how to maximize accumulation is still a bottleneck in the development of nanomedicine. Herein, a tumor vascular-targeted hybrid polymeric micelle, which has a great capacity to selectively augment the EPR effect of nanoparticles by dilating tumor blood vessels via the activity of nitric oxide (NO), is presented. Under neutral conditions, the micelle is stable, with a long blood circulation half-life due to the carboxylated poly(ethylene glycol) (PEG) layer; in mildly acidic tumor tissues, the micelle can selectively target the tumor blood vessels by the exposed cyclic Arg-Gly-Asp peptide (cRGD) peptides, which is realized with a pH-dependent hydrolysis of the monomethoxy PEG layer. Simultaneously, exposed copper ions catalyze the decomposition of endogenous NO donors, which generates NO in situ, leading to vasodilation and increased tumor vascular permeability. As a result, the accumulation of nanoparticles is significantly enhanced, and a high accumulation of doxorubicin in tumors is achieved at 48 h after injection. This high dose of therapeutic agent produces a large inhibition of tumor growth (94%) in cancer treatment, and shows no general toxicity, with 100% of the mice surviving the treatment regimen.

1. Introduction

The enhanced permeability and retention (EPR) effect, first described by Matsumura and Maeda,[1,2] has become a dominant principle in utilizing nanoparticles as drug delivery platforms for the development of nanomedicine.[3–5] The pathologically leaky vasculature and poor lymphatic drainage of tumor tissues allow nanoparticles (<400 nm) circulating in the blood to extravasate through the leaky tumor blood vessel, and enter the tumor interstitial space,[6–8] promoting the accumulation of the nanocarriers in the tumor tissues.[1,9,10] In contrast to that of the free drug, nanoparticle-based drug delivery systems can improve the therapeutic efficacy of drugs by specifically targeting tumor tissues via the EPR effect.[3] However, even with the success of EPR-based drug targeting, <10% of a systemically administered dose of nanoparticles typically accumulates in tumors after intravenous (i.v.) injection. The majority of an injected dose accumulates in the liver, spleen, and other normal organs.[11–14] A sufficiently high dosage of the systemically administered drug-loaded nanoparticles in the diseased tissues and/or cells is important for their function.[11,13] The high accumulation of nanoparticles in tumors seems to be a limiting factor in the development of nanomedicine. To address it, selectively dilating tumor blood vessels and further increasing vascular permeability will be a potent strategy for augmenting the EPR effect of nanoparticles.

In the past decade, several approaches have been explored to enhance the accumulation of drugs in tumor tissues based on the EPR effect. Various nanoparticles have been designed to improve accumulation, most of which have been developed based on the chemical or physical properties of the nanoparticles: 1) surface modification of the nanoparticles with polyethylene glycol,[15] zwitterionic groups,[16,17] and polysaccharides,[18,19] which may increase their retention in the systemic circulation and favor tumor accumulation; 2) surface modification with targeting ligands (e.g., folate,[20] hyaluronic acid,[21] peptides[22]), and switchable positive charged groups, which can increase cellular internalization[23–25]; and 3) size reductions or morphological changes of the nanoparticles, which can enhance their penetration into tumor tissues.[26–30] Despite the abilities of the above nanoparticle-modification strategies to enhance drug accumulation in tumors, more than 80% of the drug still does not produce therapeutic effects, mainly because the positively charged or ligand-modified nanoparticles can be recognized and subsequently cleared by the reticuloendothelial system (RES),[31] or because of the tumor's inherent pathological characteristics.[32] Therefore, the strategy of augmenting the EPR effect of nanoparticles by selectively dilating tumor blood vessels should be an optimal choice for enhancing drug delivery efficiency.[33]

To the best of our knowledge, this strategy, which is based on the characteristics of the tumor vessels, has rarely been employed in cancer chemotherapy. Nitric oxide (NO), as the endothelium-derived relaxing factor, has been widely reported to cause relaxation of vascular strips at concentrations below

Dr. G. Wei, Dr. Y. Wang, X. Huang, Dr. G. Yang, Dr. J. Zhao, Prof. S. Zhou
Key Laboratory of Advanced Technologies of Materials
Ministry of Education
School of Materials Science and Engineering
Southwest Jiaotong University
Chengdu, Sichuan 610031, P. R. China
E-mail: shaobingzhou@swjtu.edu.cn, shaobingzhou@hotmail.com

DOI: 10.1002/adhm.201801094

10×10^{-6} M,[34–36] and to have a strong vasodilation effect.[37] Therefore, in situ generation of NO in the tumor tissue will be an effective method to dilate blood vessels to increase vascular permeability. As we know, S-nitrosoglutathione (GSNO), S-nitrosocysteine, and S-nitrosoalbumin steadily exist in both human plasma and tissue fluids, and are known as endogenous NO donors (RSNO).[38] It has been suggested that endogenous RSNO can be used as a source of NO for vasodilation,[39,40] because RSNO can be decomposed in the presence of copper ions to generate NO;[41–44] this cycle continues until all of the RSNO species in solution are consumed.[45]

As a proof-of-concept, in this study, we developed a tumor vascular-targeted multifunctional hybrid polymeric micelle, which is capable of augmenting the EPR effect of nanoparticles by in situ production of NO to selectively dilate tumor blood vessels. As shown in **Scheme 1**a, this micelle is formed by self-assembly from the mixture of PLA-SS-PEG-PpIX-Cu-CDM-mPEG (Cu-PLEPMPss) and PCL-PEG-cRGD (PCE-cRGD) polymers, in which the poly(D, L-lactide) (PLA) and poly(ε-caprolactone) (PCL) segments form the inner core to encapsulate the anticancer drug, doxorubicin (DOX), and the poly(ethylene glycol) (PEG) segments form the outer shell. Furthermore, for the Cu-PLEPMPss copolymer, disulfide bonds (−SS−) were introduced between the PEG and PLA, giving the hybrid micelle a redox-responsive behavior. Copper ion-chelated porphyrin (PpIX-Cu) was added to the end of the PEG segment, providing a catalytic function to decompose endogenous NO donors. Subsequently, 2-propionic-3-methylmaleic anhydride (CDM)-modified methoxy polyethylene glycol (mPEG) (mPEG-CDM) was linked to the PpIX-Cu component as a pH-sensitive protective layer, in order to mask the positive charges of the micelles and avoid copper ion-catalyzed NO production in the general circulation. The grafted cRGD peptide in the PCE-cRGD copolymer can effectively target the tumor vasculature and tumor cells, on which $\alpha_v\beta_3$ integrin is overexpressed.[46–48] Scheme 1b illustrates the changes

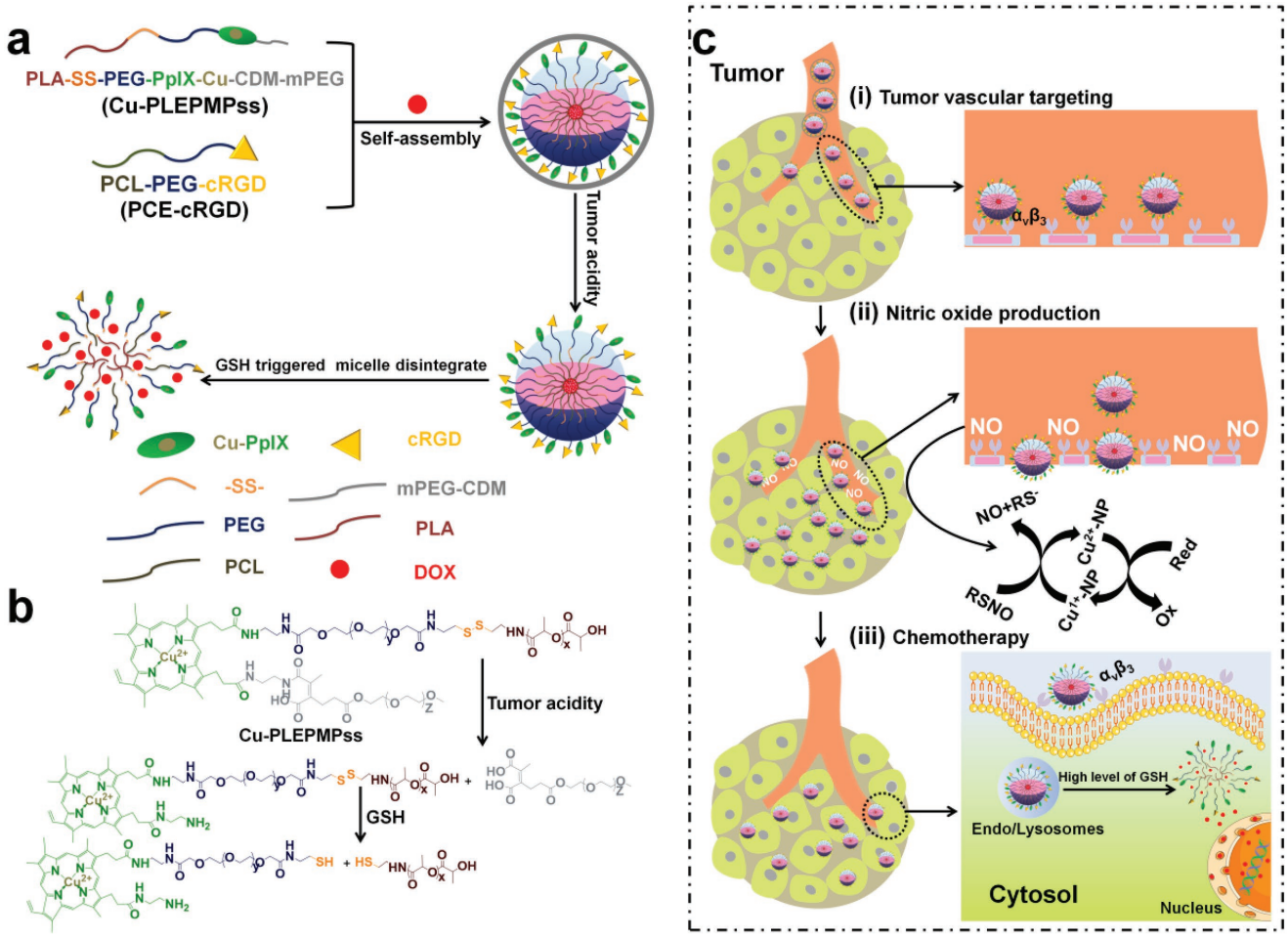

Scheme 1. Enhancing the accumulation of nanoparticles by augmenting the EPR effect. a) Schematic illustration of the formation and the pH/GSH sequential response process of the DOX@Cu-PLEPMPss-cRGD hybrid micelles. b) The chemical structure changes of the Cu-PLEPMPss copolymer in response to pH and GSH. c) Schematic of augmenting the enhanced permeation and retention (EPR) effect and chemotherapy of the micelles by 3 steps: i) selectively targeting the tumor blood vessels with the exposure of cRGD peptides as the PEG layer dissociates in the mildly acidic tumor tissue (pH 6.5), ii) in situ production of NO by the decomposition of endogenous NO donors via copper ion catalysis, resulting in blood vessel dilation, causing both high penetration and accumulation of the micelles, iii) selectively targeting the tumor cells to improve cellular internalization and GSH-triggered intracellular DOX release, leading to an enhanced chemotherapy.

in the chemical structure of Cu-PLEPMPss copolymer by sequential pH and redox changes, where the protective layer (mPEG-CDM) is deshielded from the micelles by a pH-dependent hydrolysis in the mildly acidic tumor tissues,[49] and the disulfide bonds are broken in response to high levels of glutathione (GSH) in the tumor cells.[50,51] Scheme 1c illustrates the programmed process of augmenting the EPR effect and enhancing chemotherapy of the micelles. First, the DOX-loaded hybrid micelles selectively collect in tumor blood vessels by cRGD targeting, as copper ions and cRGD peptide are exposed due to the deshielding of the mPEG-CDM layer. Second, the NO generated in situ by the copper ion-catalyzed decomposition of endogenous NO donors results in blood vessel dilation, which augments the EPR effect of the micelles. Third, the active targeting by the cRGD peptide enhances cancer cell internalization of the micelles; micelle disintegration is triggered by intracellular GSH, rapidly releasing DOX to effectively kill tumor cells.

2. Results and Discussion

The polymers, Cu-PLEPMPss and PCE-cRGD, were synthesized according to the routes as shown in **Scheme 2** and Figure S1 in the Supporting Information. The purified intermediates and final products were characterized by ^{1}H nuclear magnetic resonance (^{1}H NMR) and Fourier-transform infrared spectroscopy (FT-IR; Figure S2–14, Supporting Information). To confirm the chelation of copper ions, UV–vis analysis was further employed. From the UV–vis spectra in Figure S15a in the Supporting Information, we can see that, after conjugation with PLEss, the absorbance peaks of PpIX were almost unchanged; however, after the copper ions were chelated with the PpIX components of the PLEPss, the peaks blue-shifted, and a new peak appeared at 570 nm.[52] The results suggest that both PLEPss and Cu-PLEPss were successfully synthesized. Furthermore, approximately 90% of the PpIX was successfully grafted to the ends of the PEG segments of the PLEss copolymers, which was

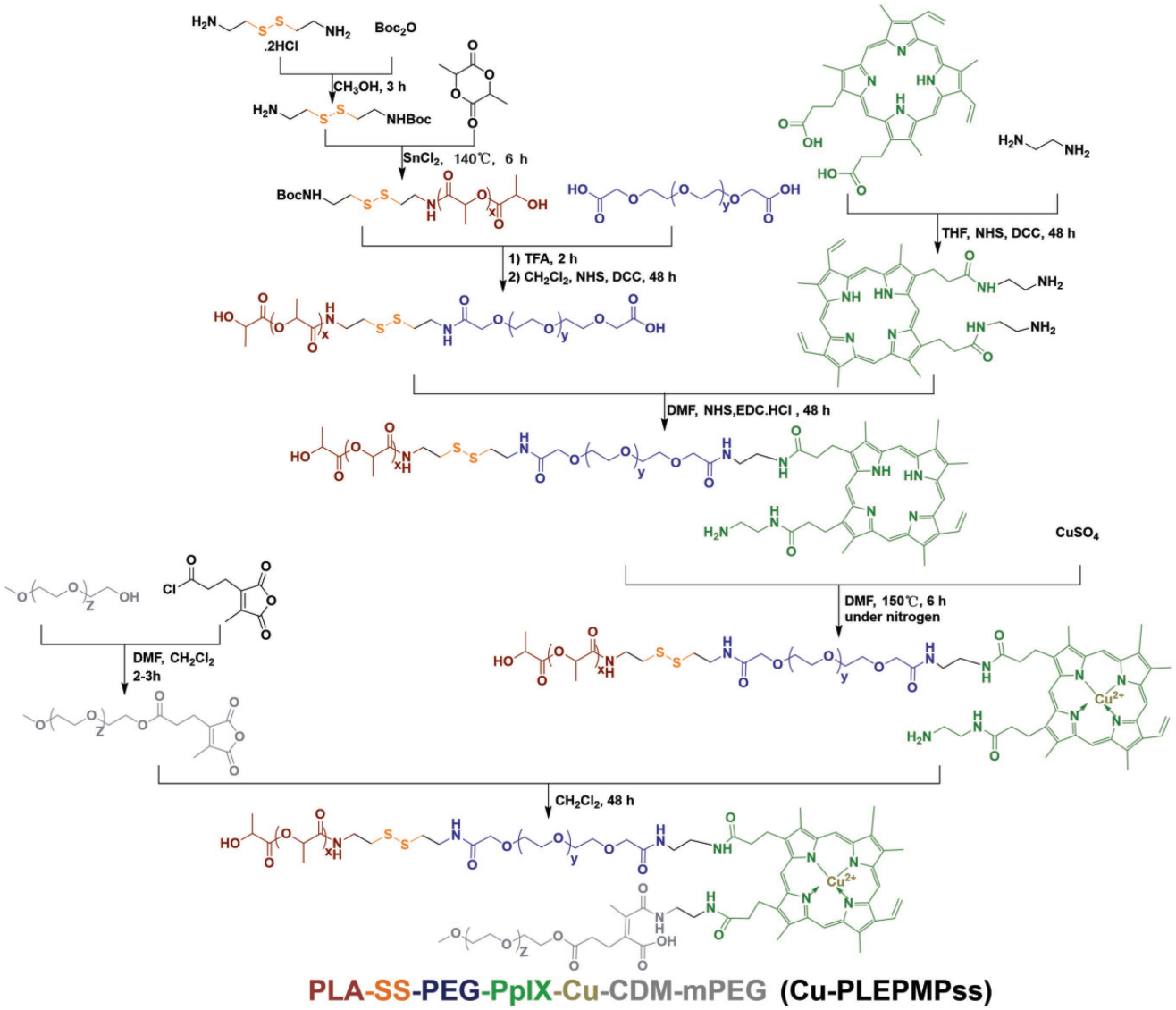

Scheme 2. Synthetic route and chemical structure of Cu-PLEPMPss copolymers.

calculated according to the UV standard curve at $\lambda = 406$ nm of the PpIX, as shown in Figure S15b in the Supporting Information; the amount of chelated copper ions in the Cu-PLEPMPss was 0.7 wt% as determined by inductively coupled plasma mass spectrometry (ICP-MS). The content of the cRGD in the PCE-cRGD polymer was determined to be 9.1 wt% by ^{1}H NMR analysis. Gel permeation chromatography revealed that the number-average molecular weights (Mn) of Cu-PLEPMPss and PCE-cRGD were 18.1 and 14.2 kDa, respectively, with a polydispersity index of 1.32 for Cu-PLEPMPss and 1.23 for PCE-cRGD.

To achieve a better targeting ability, we screened the weight ratio of the Cu-PLEPss and PCE-cRGD components in the hybrid micelles. First, we fabricated a series of blank hybrid micelles and the corresponding DOX-loaded hybrid micelles with Cu-PLEPss/PCE-cRGD (w/w) ratios of 1:0, 8:2, 6:4, 4:6, 2:8, and 0:1. The size of the blank hybrid micelles and the corresponding DOX-loaded hybrid micelles, the drug-loading content (DLC), and encapsulation efficiency (EE) are summarized in Table S1 in the Supporting Information. Second, the targeting ability of the various hybrid micelles was determined by flow cytometry. As shown in Figure S16a,b in the Supporting Information, when the amount of PCE-cRGD in the hybrid micelles was increased, using a constant concentration of DOX (5 μg mL^{-1}), the uptake of DOX by human umbilical vein endothelial cells (HUVECs) was 2.7-fold higher at a ratio of Cu-PLEPss/PCE-cRGD of 2:8 than at a ratio of 1:0 ($P < 0.01$). However, there was no significant difference among the ratios of 8:2, 6:4, 4:6, 2:8, and 0:1 ($P > 0.05$), which may be due to the fact that the cRGD peptide ligands saturate the $\alpha_v\beta_3$ receptor at the 8:2 ratio. Finally, to further verify the targeting ability of Cu-PLEPss/PCE-cRGD at a weight ratio of 8:2, mouse breast carcinoma 4T1 cells, which also have the $\alpha_v\beta_3$ integrin receptors,[53] were incubated with free DOX, DOX-loaded Cu-PLEPss (DOX@Cu-PLEPss), and DOX-loaded Cu-PLEPss-cRGD (DOX@Cu-PLEPss-cRGD) hybrid micelles with a Cu-PLEPss/PCE-cRGD ratio of 8:2. The flow cytometry results in Figure S16c,d in the Supporting Information demonstrate that the amount of DOX in cells incubated with DOX@Cu-PLEPss-cRGD hybrid micelles was ≈5-fold higher than that with DOX@Cu-PLEPss micelles, but DOX@Cu-PLEPss-cRGD hybrid micelles was internalized by cells via cRGD receptor-mediated endocytosis as demonstrated by the diminished intracellular fluorescence intensity of DOX when cells were pretreated by molecular cRGD. This is likely attributed to the fact that cRGD peptide can promote cellular internalization. The result also indicates that hybrid micelles with a Cu-PLEPss/PCE-cRGD ratio of 8:2 have the best targeting ability. Thus, these hybrid micelles were selected for subsequent studies.

To confirm whether the copper ion-chelated micelles have the ability to catalyze GSNO decomposition to generate NO, the Cu-PLEPss micelles were mixed with 10×10^{-6} M GSNO and 10×10^{-6} M GSH in aqueous solution at 37 °C, and the generated NO was measured by real-time detection with a chemiluminescence NO analyzer (NOA). **Figure 1**a shows that the rate of NO generation was stable at 8×10^{-10} mol min^{-1} after the addition of Cu-PLEPss micelles, but we detected no generation after the addition of PLEPss micelles without copper ions. These results suggest that the NO generation is strongly dependent on the copper ion-catalyzed decomposition reaction of GSNO.[37] To further quantitatively analyze the NO generation, a Griess kit was used to determine the NO concentration in the phosphate-buffered solution (PBS) containing 10×10^{-6} M GSNO and 10×10^{-6} M GSH or in the F12 medium containing 10% fetal bovine serum (FBS), 10×10^{-6} M GSNO and 10×10^{-6} M GSH for 1 and 6 h after the addition of micelles. As shown in Figure 1b, for the Cu-PLEPss group, there was 1.3×10^{-6} M NO generated after an incubation of 1 h and 3.1×10^{-6} M NO generated after an incubation of 6 h. Moreover, the NO concentration in serum-containing media has no significantly different from that in the PBS solution after incubated for same time. Theses concentration levels of NO can effectively promote vasodilation.[36,37] For the PLEPss group, NO was little detected, even after 6 h of incubation. These results indicate that the generated NO concentration is strongly dependent on the presence of copper ions and the incubation time.

We further investigated whether the NO can be generated in vascular endothelial cells by copper ion catalysis. To simulate the in vivo microenvironment, HUVEC were incubated with F12 medium containing 10% (v/v) FBS with 10×10^{-6} M GSNO and 10×10^{-6} M GSH for 24 h. Afterward, the medium was replaced with fresh medium, the cells were treated with Cu-PLEPss micelles or Cu-PLEPss-cRGD hybrid micelles, and the generation of NO was detected using a fluorescent probe (i.e., DAF-FM DA) by fluorescence microscopy and flow cytometry. The fluorescence intensity of intracellular NO levels in the HUVEC was significantly increased in a concentration-dependent manner by treatment with 10–250 μg mL^{-1} of Cu-PLEPss micelles (Figure 1c1). Moreover, the fluorescence intensity of the cells treated with Cu-PLEPss-cRGD was much higher than that with Cu-PLEPss at the same copper ion concentration and incubation time, demonstrating that the cRGD ligand can improve cell internalization (Figure 1c2). Additionally, the fluorescence intensity increased in a time-dependent manner (Figure 1c2). These results are consistent with the flow cytometry results in Figure 1d,e, demonstrating that the NO was indeed produced inside the vascular endothelial cells due to the fact that the copper ion-chelated micelles can catalyze decomposition of the NO donor (GSNO). The cell viability was analyzed after HUVEC were incubated with PLEPss, Cu-PLEPss micelles, or Cu-PLEPss-cRGD hybrid micelles at different concentrations in the F12 medium containing 10% FBS, 10×10^{-6} M GSNO, and 10×10^{-6} M GSH. Figure S17 in the Supporting Information shows that the cell viability in all groups was >90% after incubation with 10–250 μg mL^{-1} of micelles for 24 h, indicating that the catalytic production of NO at such micellar concentrations was not cytotoxic to the cells, and that the blank micelles showed excellent cytocompatibility.

To investigate whether the catalytic production of NO at this concentration is capable of killing the 4T1 tumor cells incubated with Cu-PLEPss-cRGD hybrid micelles, the cell viability determined by live/dead staining and AB assay in Figure S18 in the Supporting Information shows that >90% cells grow healthily for 6, 12, or 24 h, indicating that the catalytic production of NO at such concentration almost cannot kill tumor cells.

To avoid the catalytic reaction between copper ions and GSNO during blood circulation and to prolong the circulation time of the micelles, mPEG-CDM was attached to the Cu-PLEPss to mask both the positive charge and the copper ions

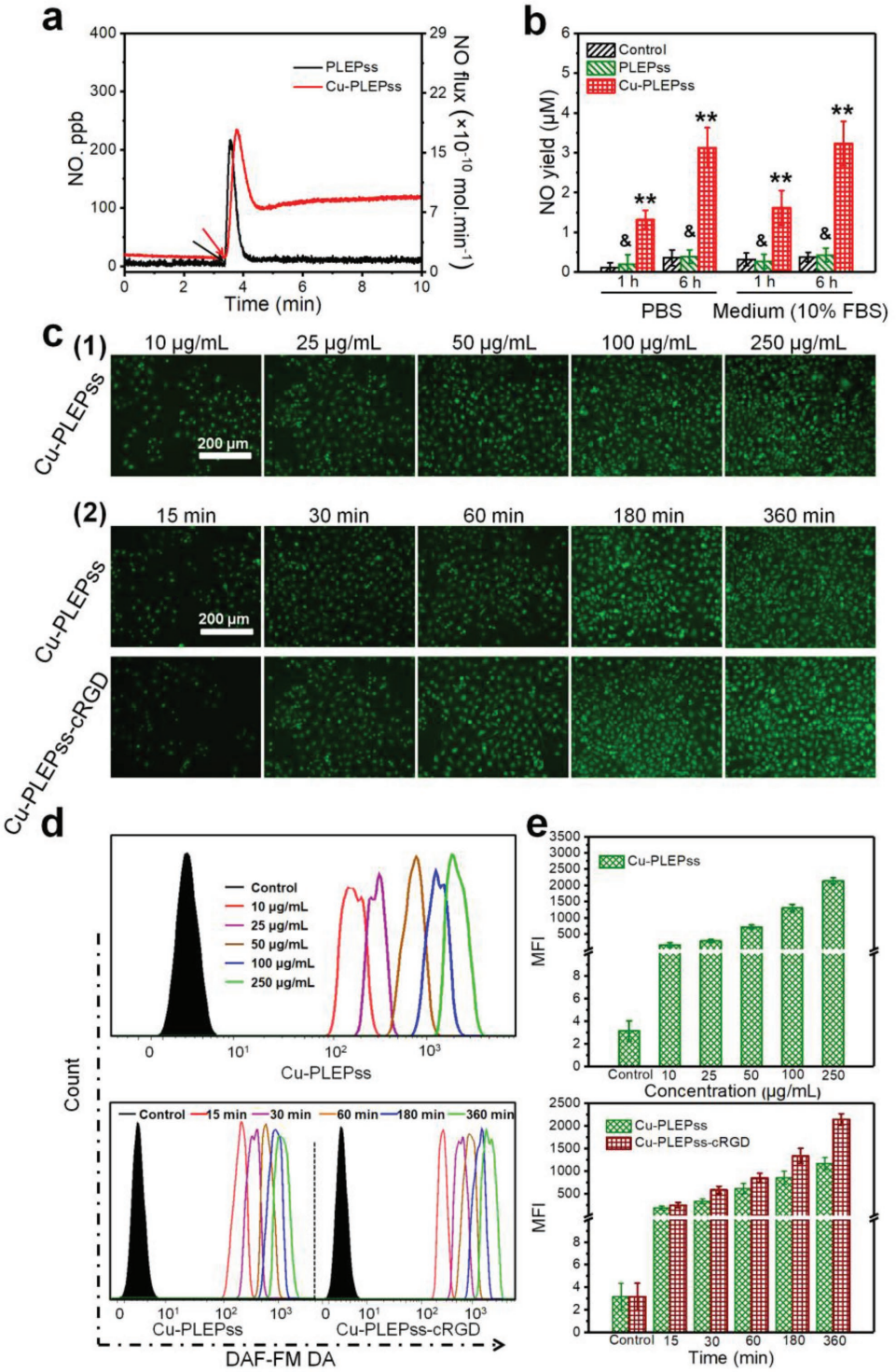

Figure 1. The analysis of NO generation by copper ion catalysis. a) Chemiluminescence NOA for real-time detection of NO generation in 10 min (the red arrow indicates the time of Cu-PLEPss addition, and the black arrow indicates the time of PLEPss addition) and b) Griess assay for determining the amount of NO generated by adding Cu-PLEPss or PLEPss in PBS solution (pH 7.4) or containing 10×10^{-6} M GNSO and 10×10^{-6} M GSH at 37 °C or in 10% FBS solution (pH 7.4) containing 10×10^{-6} M GSNO and 10×10^{-6} M GSH at 37 °C for 1 and 6 h. PBS or 10% FBS solution as a control ($n = 3$). c) Fluorescence microscopy images of intracellular NO generated in HUVEC after treatment with Cu-PLEPss micelles at 10–250 μg mL^{-1} for 3 h (1) and with Cu-PLEPss micelles or Cu-PLEPss-cRGD hybrid micelles at a copper ion concentration of 0.7 μg mL^{-1} from 15–360 min (**2**). d) Flow cytometry analysis and e), the corresponding quantitative evaluation of intracellular NO in HUVEC cells after treated with Cu-PLEPss micelles or Cu-PLEPss-cRGD hybrid micelles. The untreated cells were used as the control ($n = 3$). The values were expressed as mean ± SD. $^{**}p < 0.01$ or $^{\&}p > 0.05$.

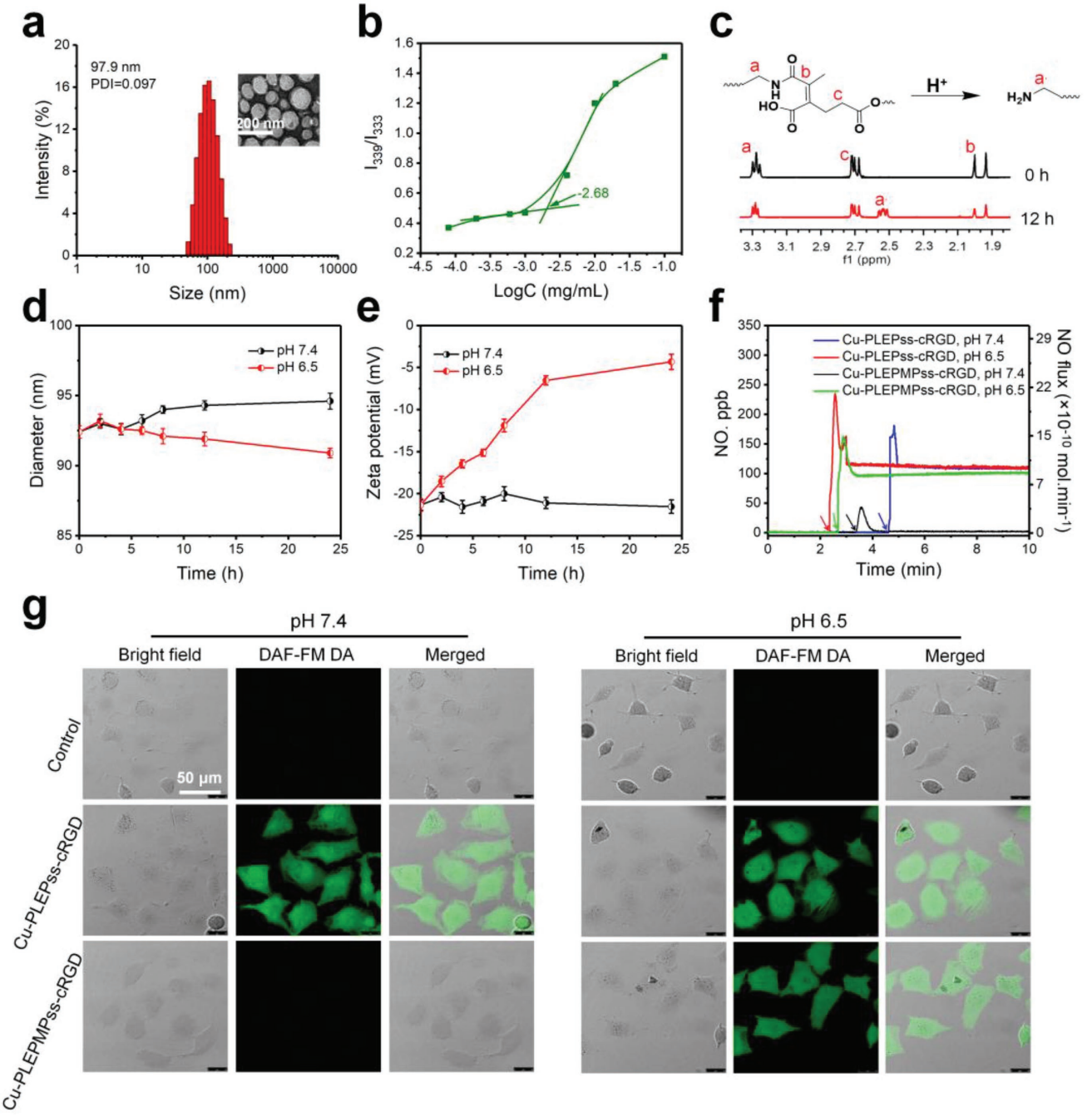

Figure 2. The in vitro NO generation induced by the nanoparticles. a) Hydrodynamic size distribution and the inserted TEM image of Cu-PLEPMPss-cRGD hybrid micelles. b) The CMC derived from the plot of I_{339}/I_{333} ratio versus copolymer concentration using pyrene as a probe. c) ^{1}H-NMR spectra of the degradation products after Cu-PLEPMPss incubated at pH 6.5 for 0, 12 h and the removal of the mPEG segment. d) Diameter, and e) zeta potential changes of Cu-PLEPMPss at pH 7.4 or 6.5 ($n = 3$). f) NO generated by adding Cu-PLEPss-cRGD and Cu-PLEPMPss-cRGD hybrid micelles in PBS solution (pH 7.4 or 6.5) containing 10 and 10×10^{-6} M GSH at 37 °C (different colored arrow indicates the time of corresponding micelle addition). The untreated cells were used as the control. g) Confocal images of the HUVEC cells for cells alone, Cu-PLEPss-cRGD, and Cu-PLEPMPss-cRGD hybrid micelles after incubation at pH 7.4 or 6.5 for 12 h. The green fluorescence was derived from DAF-FM DA. The untreated cells were used as the control.

to obtain the pH-sensitive Cu-PLEPMPss polymer; this was further blended with PCE-cRGD to form Cu-PLEPMPss-cRGD hybrid micelles. The characterizations of the Cu-PLEPMPss-cRGD hybrid micelles are shown in Figure S19 in the Supporting Information and **Figure 2**a,b. The results of dynamic light scattering (DLS) measurements indicated that the average diameters were ≈92.9 nm for Cu-PLEPMPss micelles, 99.0 nm for PCE-cRGD micelles, and 97.9 nm for Cu-PLEPMPss-cRGD hybrid micelles. The inset transmission electron microscopy (TEM) image in Figure 2a also shows that the micelles have

a good spherical shape with a size of ≈90.0 nm. It has been demonstrated that small nanoparticles (<400 nm) are more likely to extravasate from leaky vasculature into the tumor interstitium.[54] Therefore, these micelles, with a size of approximately 100 nm, possess great potential for increasing intratumoral delivery. The critical micelle concentration (CMC) values of the Cu-PLEPMPss, PCE-cRGD, and Cu-PLEPMPss-cRGD micelles were 4.365×10^{-3}, 1.349×10^{-3}, and 2.089×10^{-3} mg L^{-1}, respectively. Such low CMC values ensure that these micelles will remain stable, even when diluted within the body.

To determine whether the mPEG-CDM layer can dissociate from the Cu-PLEPMPss micelles in mildly acidic conditions, the micelles were dispersed in an aqueous solution at pH 6.5 for 12 h. The solution was then freeze-dried and the products were analyzed by ^{1}H NMR. Figure 2c clearly shows that a new chemical shift at 2.55 ppm (peak a′) appeared, which is a characteristic resonance of methylene protons adjacent to an amino group, and that the resonance intensity of the protons adjacent to the amide bond (peak c) decreased after the 12 h incubation. The result is almost in agreement with that of a previous report,[49] suggesting that the amide bond is sensitive to the acidic environment and pH-dependent hydrolysis. Calculated from the relative integration, nearly 50% of the linkers (amide bonds) were cleaved after the 12 h incubation at pH 6.5. We also studied the influence of mPEG detachment on both the size and zeta potential of the Cu-PLEPMPss micelles, which were incubated at both pH 6.5 and 7.4. The DLS results in Figure 2d indicate that little change in size occurred under the two pH conditions. However, the zeta potential displayed a constantly negative surface charge of approximately –21.34 mV at pH 7.4. After incubation at pH 6.5 for 24 h, the zeta potential changed to approximately –4.32 mV (Figure 2e), indicating the partial removal of the mPEG corona to expose the copper ions.

To verify whether the Cu-PLEPMPss-cRGD hybrid micelles can promote NO generation through a catalytic reaction between copper ions and GNSO, HUVECs were incubated with the micelles. The group treated with Cu-PLEPss-cRGD hybrid micelles without pH sensitivity was used as a control. All of the micelles were pretreated at pH 7.4 or 6.5 for 24 h. After 1 h of incubation, the intracellular NO generated was detected using a fluorescent probe (i.e., DAF-FM DA) and visualized by confocal laser scanning microscopy (CLSM). As shown in Figure 2g, the intracellular NO was nearly constant in the Cu-PLEPss-cRGD group due to the exposure to copper ions, regardless of the pretreatments at different pH values. For the Cu-PLEPMPss-cRGD group pretreated at pH 7.4, intracellular NO could not be detected due to the shielding of copper ions by the mPEG-CDM component. However, after pretreatment at pH 6.5, the intracellular NO sharply increased with the exposure to copper ions due to the deshielding of the mPEG-CDM. The chemiluminescence NOA also quantitatively confirmed the rate of NO generation induced by Cu-PLEPss-cRGD and Cu-PLEPss-cRGD hybrid micelles through the copper ion catalytic reaction (Figure 2f).

The stability and redox sensitivity of the Cu-PLEPMPss-cRGD hybrid micelles were further investigated. From the UV–vis spectra of the Cu-PLEPMPss-cRGD hybrid micelles treated at pH 7.4 and 6.5 for 24 h, it can be seen that the two curves almost overlap (Figure S20a, Supporting Information), demonstrating that the amount of copper ions in the Cu-PLEPMPss-cRGD was similar in the two conditions; therefore, the chelation of the copper ions is stable in mildly acidic environments, and is also stable in H_2O, PBS or cell culture medium (containing 10% FBS, v/v) at 37 °C (Figure S21, Supporting Information). In addition, the ultraviolet absorption changes of the Cu-PLEPMPss-cRGD hybrid micelles after incubation in H_2O, PBS, or cell culture medium (containing 10% FBS, v/v) were also investigated. Similarly, it can be seen that there is no obvious difference in their size after incubation for 24 h (Figure S20b, Supporting Information), suggesting that the micelles have a good stability in blood.

To further evaluate the redox sensitivity of the Cu-PLEPMPss-cRGD hybrid micelles, DLS was performed to measure their average size in PBS (pH 7.4) with different GSH concentrations (10×10^{-6} M and 10×10^{-3} M). The results show that the size distribution of the micelles changed from an original, unimodal peak to a wide peak over time with 10×10^{-3} M GSH (Figure S20c, Supporting Information), which resulted from the cleavage of the disulfide bonds of the Cu-PLEPMPss.

To further evaluate the drug release behaviors, the DOX@Cu-PLEPMPss-cRGD hybrid micelles were dispersed in PBS (pH 7.4 or 6.5, containing 10×10^{-6} M or 10×10^{-3} M GSH) or acetate buffer saline (ABS, pH 5.0, containing 10×10^{-6} M or 10×10^{-3} M GSH), and dialyzed against the corresponding dispersion medium at 37 °C in the dark for predetermined times. The DOX-loaded PLEPMPss, Cu-PLEPMPss, and Cu-PLEPMPss-cRGD hybrid micelles have particle sizes of 100 nm and a good DLC of 5% (Table S2, Supporting Information). The drug release profile (Figure S20d, Supporting Information) of DOX@Cu-PLEPMPss-cRGD hybrid micelles shows that there was only 10% drug release in 72 h at pH 7.4 with 10×10^{-6} M GSH, which is similar to the blood environment, suggesting that the micelles are highly stable in blood. However, the quantity of DOX cumulative release increased to ≈19% at pH 6.5 or 5.0 with 10×10^{-6} M GSH; this was probably due to the protonation of the glycosidic amine of DOX at low pH, which enhanced the diffusion of DOX from the polymeric micelles.[55] and it was further proved that the DOX@Cu-PLEPMPss-cRGD hybrid micelles could maintain a good nuclear-shell structure in mildly acidic environment. A rapid release of DOX was initiated at pH 7.4 or 5.0 with 10×10^{-3} M GSH by 6 h, and there was a sharp increase in drug release with 10×10^{-3} M GSH to 79% at pH 7.4 and 84% at pH 5.0 within 72 h. The reason for this observation is mainly attributed to the disassembly of the micelles upon disulfide bond cleavage with high levels of GSH.[56] Therefore, the DOX-loaded hybrid micelles have a great stability in blood circulation but an accelerated DOX release in cytoplasm.

Live/dead staining and Alamar Blue (AB) assays were adopted to assess the cytocompatibility of blank Cu-PLEPMPss-cRGD hybrid micelles at different concentrations. **Figure 3**a,b shows that the cell viability was >90% for HUVEC and 4T1 cells after incubation with the micelles at 10–250 μg mL^{-1} for 24 h, indicating that the blank hybrid micelles had excellent cytocompatibility. Figure 3c shows that the cell viability of 4T1 cells cultured with DOX@Cu-PLEPMPss or DOX@Cu-PLEPMPss-cRGD hybrid micelles at pH 6.5 was concentration dependent. The IC_{50} value (i.e., the concentration resulting in

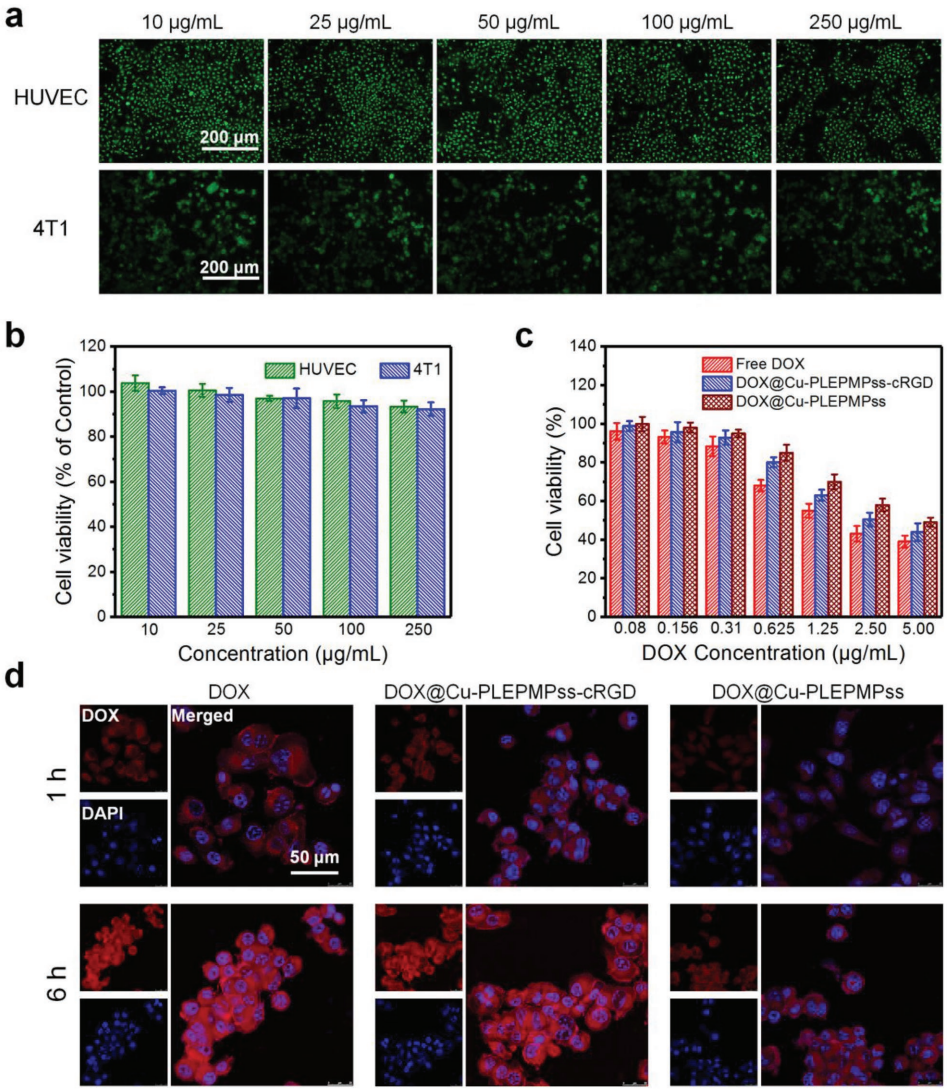

Figure 3. In vitro cytotoxicity assay and subcellular localization. a) Fluorescence images of HUVEC cells and 4T1 cells after treated with blank micelles at different concentrations for 24 h. The live cells were stained green. b) Cell viability of HUVEC cells and 4T1 cells after incubation with blank micelles at different concentrations for 24 h ($n = 3$). c) Cytotoxicity of 4T1 cells treated by free DOX and DOX-loaded micelles as a function of DOX concentration ($n = 3$). d) Confocal images of 4T1 cells after incubation with free DOX and various DOX-loaded micelles for 1 and 6 h. The nuclei were stained blue with DAPI and DOX visualized with red fluorescence.

50% cell inhibition) for DOX@Cu-PLEPMPss micelles was 3.738 μg mL^{-1}, but the IC_{50} value for DOX@Cu-PLEPMPss-cRGD micelles was 2.884 μg mL^{-1}, which is similar to that of free DOX (IC_{50} = 2.064 μg mL^{-1}). This suggests that the cRGD peptide targeting ligand enhances cellular internalization through integrin $\alpha_v\beta_3$ receptor-mediated endocytosis. This can also be confirmed by the confocal images in Figure 3d, where 4T1 cells treated with DOX@Cu-PLEPMPss-cRGD hybrid micelles show more red fluorescence than those treated with DOX@Cu-PLEPMPss micelles at both 1 and 6 h (Figure 3d).

NO functions to dilate blood vessels. We investigated whether treatment with the copper ion-chelated micelles could lead to vasodilation of tumor vasculature. By using dye-labeled anti-CD31 antibody, immunofluorescence images of tumor blood vasculature was obtained with frozen cross-sections of tumor tissues that had been treated with saline, PLEPMPss-cRGD hybrid micelles, Cu-PLEPMPss micelles, or Cu-PLEPMPss-cRGD hybrid micelles According to previous reports, dilated blood vessels can be characterized by their margins.[57] The images in **Figure 4**f show that the dilated blood vessels as characterized by the complete margins was much thinner after Cu-PLEPMPss-cRGD hybrid micelles treatment than that in the PLEPMPss-cRGD hybrid micelles treated group (white arrows indicate dilated blood vessels), suggesting that the copper ions are the key factors in the dilation of blood vessels due to endogenous NO generation by in situ copper ion catalysis. Furthermore, the number of dilated blood vessels treated with Cu-PLEPMPss-cRGD hybrid micelles was much greater than that treated with Cu-PLEPMPss micelles (Figure S22, Supporting Information, white arrows indicate dilated blood vessels). This can be ascribed to the fact that the cRGD targeting of Cu-PLEPMPss-cRGD hybrid micelles increases the

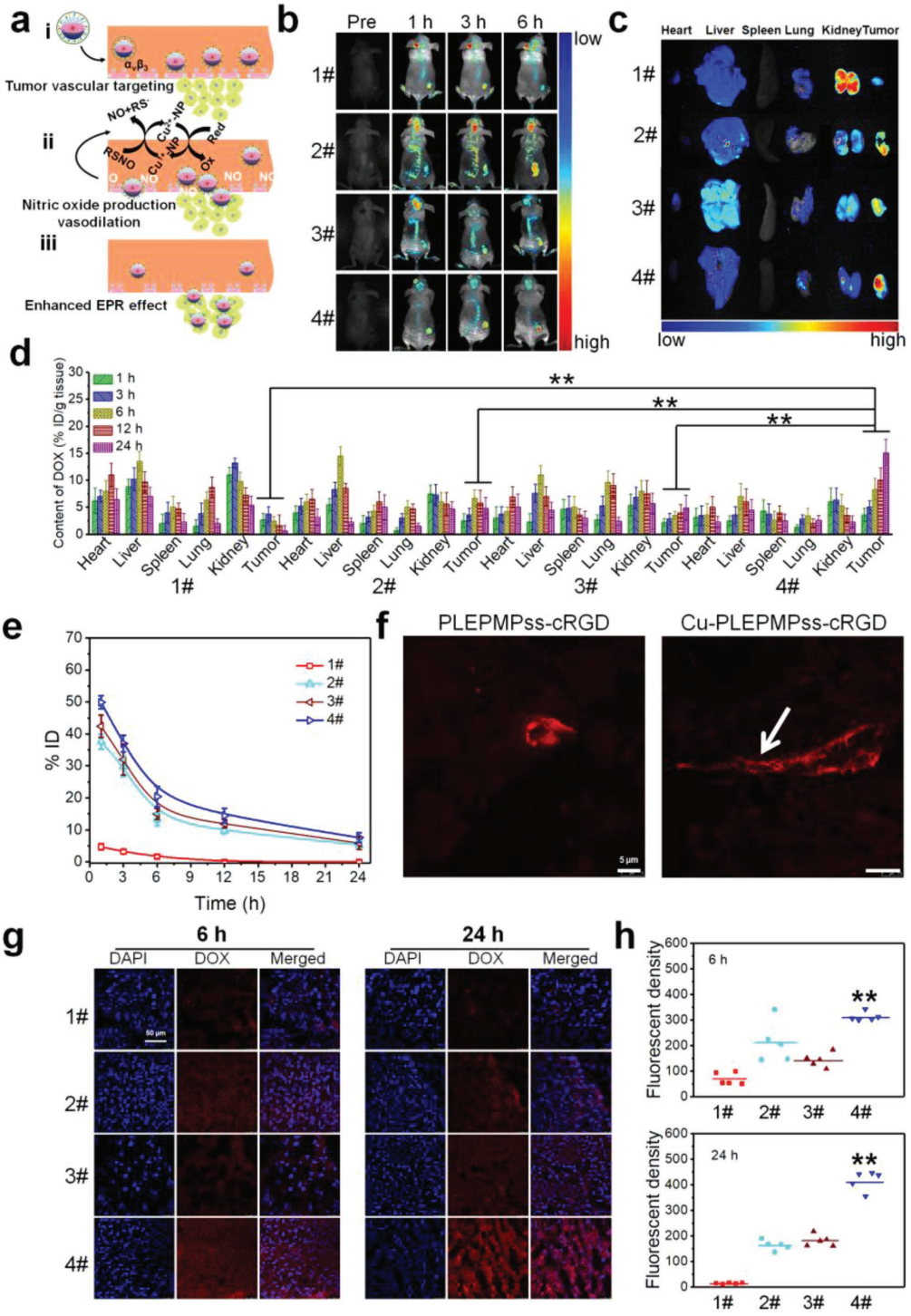

Figure 4. In vivo and ex vivo biodistribution analyses. a) The accumulation of DOX@Cu-PLEPMPss-cRGD hybrid micelles in the tumor, which could i) target the tumor blood vessels with the exposure of cRGD peptide, ii) produce NO in situ by copper ion catalysis, and iii) enhance micelle penetration due to vasodilatation caused by NO. b) In vivo DOX biodistribution of various DOX formulations determined by fluorescent imaging in 4T1 tumor-bearing nude mice (dose: 2 mg DOX kg^{-1} body weight). c) Ex vivo DOX biodistribution in major organs and tumors examined 6 h postadministration. d) Quantitative analysis of the DOX distribution in major organs and tumors ($n = 3$). e) Pharmacokinetic profiles of total DOX, post-i.v. injection, of various drug formulations ($n = 3$). f) Confocal images of tumor blood vessels of frozen tumor slices stained by anti-CD31 antibody after treatment by the micelles with or without copper ions for 6 h. White arrows indicate dilated blood vessels. g) Confocal images of tumor frozen sections, which were excised from different treatment groups at 6 and 24 h. Blue, DAPI-stained cell nuclei; Red, DOX or DOX-loaded micelles. h) Quantitative analysis of the fluorescence density of DOX in 4T1 tumor frozen sections by ImageJ ($n = 5$). 1#: free DOX. 2#: DOX@PLEPMPss-cRGD hybrid micelles. 3#: DOX@Cu-PLEPMPss micelles. 4#: DOX@Cu-PLEPMPss-cRGD hybrid micelles. The values were expressed as mean ± SD. $^{**}p < 0.01$.

accumulation of the micelles in tumor blood vessels, causing more NO generation. The results demonstrate that the tumor blood vessels can be selectively dilated by the endogenous copper ion-catalyzed NO generation, resulting in the augmented EPR effect of the micelles.

To directly evaluate the active targeting and accumulation of the micelles in vivo, the various DOX formulations were injected into 4T1 tumor-bearing nude mice at a dose of 2 mg DOX/kg body weight, and the fluorescence intensity of DOX at different sites of the body was monitored at different time points by ex vivo imaging. Figure 4a shows the active targeting and accumulation of DOX@Cu-PLEPMPss-cRGD hybrid micelles in tumor tissue, which has the following special functions: i) selectively targeting the tumor blood vessels, ii) in situ production of NO by copper ion-catalysis of endogenous NO donors, and iii) augmentation of the EPR effect of the micelles via vasodilatation caused by NO. Figure 4b shows that the DOX fluorescence intensity of the free DOX group was stronger at the tumor site compared to that of the other groups at 1 h postinjection due to the fast diffusion of the small DOX molecules, but it declined after 3 h of treatment. In contrast, the DOX fluorescence intensity of DOX-loaded micelles gradually increased at the tumor site, being much stronger in the DOX@Cu-PLEPMPss-cRGD group than in the DOX@PLEPMPss-cRGD group and DOX@Cu-PLEPMPss group. All the results demonstrate that the DOX-loaded micelles have a long half-life in the blood, and the copper ion-chelated micelles can penetrate into tumor tissues more easily by the NO-induced augmented EPR effect than the micelles without copper ions. Six hours after injection, major organs (heart, liver, spleen, lung, kidneys) and tumor were excised to further study the biodistribution of the various DOX formulations in vivo. In Figure 4c, the strongest DOX fluorescence intensity in the tumor can be seen in the DOX@Cu-PLEPMPss-cRGD group; moreover, little DOX fluorescence was found in normal tissues, confirming the targeting ability of the cRGD peptide and the NO-induced augmented EPR effect.

To further investigate the biodistribution and pharmacokinetics of DOX over a longer time in vivo, BALB/c mice were intravenously injected with the various DOX formulations at a dose of 2 mg DOX/kg body weight. The plasma was collected after injection at predetermined time points (1, 3, 6, 12, and 24 h), and then the quantity of DOX was measured with a fluorescence spectrometer. Figure 4e shows the blood clearance curves of the various DOX formulations, and there were significant differences in the pharmacokinetic profiles of free DOX and the various DOX-loaded micelles. Table S3 in the Supporting Information summarizes the pharmacokinetic parameters, which were calculated by fitting the blood drug concentration to a two-compartment model. Free DOX was easily eliminated from the blood with a rapid elimination half-life ($t_{1/2\beta}$ = 1.39 h). However, after it was loaded in polymer micelles, the elimination of DOX was significantly slower ($t_{1/2\beta}$ = 11.81 h for DOX@PLEPMPss-cRGD hybrid micelles, 11.38 h for DOX@Cu-PLEPMPss micelles, and 12.20 h for DOX@Cu-PLEPMPss-cRGD hybrid micelles). The results suggest that these DOX-loaded micelles have a long blood circulation due to the effect of the PEG.[58] Next, we quantitatively analyzed the DOX distribution in major organs and tumors for the various DOX formulations. As shown in Figure 4d, for the free DOX group, DOX mainly accumulated in the liver, lung, and kidneys, with the lowest accumulation in tumors among all of the groups, 24 h after injected, which was consistent with the ex vivo imaging (Figure 4c). In contrast, the amount of DOX accumulated in tumors increased in the DOX-loaded micelle groups. In particular, the amount of DOX in the DOX@Cu-PLEPMPss-cRGD group was markedly decreased in normal organs, but significantly enhanced in a time-dependent manner in tumor tissues. Twenty-four hours after injection, the cumulative content of DOX in the tumor was 15.1% ID/g, which is 3.1-fold greater than that of the other two DOX-loaded micelles (4.9% ID/g for DOX@PLEPMPss-cRGD hybrid micelles without copper ions and 4.8% ID/g for DOX@Cu-PLEPMPss micelles without active targeting ligands). This DOX content of 15.1% ID/g in the tumor is also higher than that reported previously.[11,13] The results are in good agreement with the in vivo and ex vivo DOX fluorescence imaging, also demonstrating the targeting ability of the cRGD peptide, and the NO-induced augmented EPR effect of vasodilation (Figure 4f). In addition, the biodistribution of Cu-PLEPMPss and Cu-PLEPMPss-cRGD at 6 and 24 h after i.v. injection into 4T1 tumor-bearing mice was also determined by copper ion measurement in various organs and tissues via inductively coupled plasma optical emission spectrometer (ICP-OES) analysis. The result (Figure S24, Supporting Information) shows that the amount of copper ion in the DOX@Cu-PLEPMPss-cRGD group was also significantly enhanced in a time-dependent manner in tumor tissues. Twenty-four hours after injection, the cumulative content of copper ion in the tumor was 13.1% ID/g, which also is ≈3-fold greater than that of the DOX@Cu-PLEPMPss group without active targeting ligands (4.2% ID/g). The effective enrichment of copper ions in the tumor ensured that endogenous RSNO could be catalyzed to generate NO for vasodilation.

To further confirm the effective DOX level in tumors treated with DOX@Cu-PLEPMPss-cRGD hybrid micelles, the amount of DOX accumulation was detected at 36 and 48 h after injection (Figure S23, Supporting Information). The results show that the micelles can be sustained in the tumor, and the DOX concentration even rose to 17.8% ± 2.3 ID/g at 48 h after injection. The reason for the high accumulation can be ascribed to that the copper ions catalyze the decomposition of the endogenous NO donors (RSNO) in situ to produce NO, dilating tumor blood vessels, and, in turn, causing an increase in vascular permeability and augmenting EPR effect, which can significantly enhance the accumulation of the DOX-loaded micelles in tumor tissues. This high dosage of therapeutic agent in the tumor tissue is critical in enhancing antitumor efficiency. To further evaluate the accumulation of these DOX formulations, the frozen sections of tumor tissues were measured by CLSM (Figure 4g). The result also indicated that the strongest red fluorescence occurred in tumor tissues in the DOX@Cu-PLEPMPss-cRGD group and that the fluorescence intensity increased in a time-dependent manner. The quantitative analysis in Figure 4h is essentially consistent with that in Figure 4d. The results confirm that the DOX@Cu-PLEPMPss-cRGD hybrid micelles preferentially accumulate in the tumor because of the cRGD targeting and the NO-induced augmented EPR effect.

The in vivo antitumor effect of DOX@Cu-PLEPMPss-cRGD hybrid micelles was further examined in BALB/c mice bearing 4T1 xenograft tumors. After a 21 d treatment, no obvious body weight changes were observed in all groups, except in the free DOX group (**Figure 5**a), indicating negligible systemic toxicity of the DOX-loaded micelles. Meanwhile, from the tumor growth curves in Figure 5b, it can be seen that the DOX-loaded micelle groups, especially the DOX@Cu-PLEPMPss-cRGD group produces a greater decrease in tumor growth, resulting in a relative tumor volume of only 0.4 on day 21. However, owing to the short half-life of DOX in blood,[59] the relative tumor volume of the free DOX group was the largest among all DOX-treated groups, which was 14.5-fold greater than that of the DOX@Cu-PLEPMPss-cRGD group on day 21. Additionally, the relative tumor volumes of DOX@PLEPMPss-cRGD without copper ions and DOX@Cu-PLEPMPss without cRGD were, respectively, 10.8-fold and 10.4-fold greater than that of the DOX@Cu-PLEPMPss-cRGD hybrid micelles on day 21. All these results demonstrate that this highly effective cancer treatment results from a high accumulation of nanomedicine in the tumor, which is attributed to the augmented EPR effect and cRGD targeting. The images (Figure 5c) and tumor weights (Figure 5d) of the excised solid tumors on day 16 further confirmed the anticancer effect. The average tumor weight in the DOX@Cu-PLEPMPss-cRGD group was only 0.03 g, which is 30-fold less than that of the free DOX group (0.9 g), and >20-fold less than that of the DOX-loaded micelle group without cRGD targeting (0.8 g) or group without copper ions (0.7 g). The inhibition rate (IR) of tumor growth was also calculated on day 16 to further evaluate the therapeutic effect. In Figure 5e, in contrast to all DOX-loaded micelles, free DOX had the lowest IR (56%). However, the IR of the DOX@PLEPMPss-cRGD hybrid micelles was calculated to be 94%, which is the highest among all of the DOX nanoformulations.

Moreover, the survival rate of mice in the DOX@Cu-PLEPMPss-cRGD group was the highest (100%) among all groups (Figure 5f), implying the safest treatment. In vivo toxicity of nanoparticles is another crucial parameter for preclinical evaluation. General body toxicity was further evaluated by hematoxylin and eosin (H&E) staining of the major organs (e.g., heart, liver, spleen, lung, and kidney treated by all of the DOX formulations). The H&E-stained images in Figure S25 in the Supporting Information show that, except for cardiotoxicity in the free DOX group, there were no appreciable histological changes and undetectable adverse effects (e.g., inflammatory response or necrosis) in the main organs in all micelle groups, indicating excellent biocompatibility in vivo. Moreover, no obvious toxicities induced by Cu-PLEPMPss-cRGD hybrid blank micelles were observed, as shown in the blood biochemistry and hematology analysis (Figure S26, Supporting Information). Therefore, the DOX@Cu-PLEPMPss-cRGD hybrid micelle is a good nanoformulation for cancer therapy because it possesses both high antitumor efficacy and low systemic toxicity.

Furthermore, to determine the mechanism of the enhanced tumor suppression by DOX@Cu-PLEPMPss-cRGD hybrid micelles, the expression of the proapoptotic protein, caspase-3, in the tumor tissues was evaluated by Western blot analysis. As illustrated in Figure 5g,h, compared to that of the other five groups, an enhanced expression of caspase-3 protein was found in the DOX@Cu-PLEPMPss-cRGD group, implying increased apoptosis. Additionally, histological analyses of the tumor tissues on day 16 were performed to evaluate antitumor activity at the cellular level. In Figure 5i, the H&E-stained images clearly show that, compared with that of the saline and blank micelle groups, the DOX-loaded micelle groups, especially the DOX@Cu-PLEPMPss-cRGD group, had significant nuclear shrinkage and fragmentation, which suggested that it had the best antitumor efficacy. Similarly, the terminal deoxynucleotidyl transferase dUTP nick end labeling (TUNEL)-stained images also show that the DOX@Cu-PLEPMPss-cRGD group exhibited remarkable antitumor activity, as indicated by the largest area of cell apoptosis. Additionally, to further verify the antiproliferative ability, the expression of Ki67 (a cellular marker) was examined. Ki67-stained images show a lower expression in tumors treated with DOX@Cu-PLEPMPss-cRGD hybrid micelles compared to that of the other groups, indicating that the hybrid micelles with copper ions had the best efficacy in suppressing tumor cell proliferation and promoting antitumor effects. Therefore, all of the results demonstrate that the DOX@Cu-PLEPMPss-cRGD hybrid micelles have the best anticancer effects due to the high accumulation of therapeutic agent in tumor tissue by the augmented EPR effect.

3. Conclusions

In summary, we have presented a new tumor vascular-targeted hybrid polymeric micelle, which possesses a great capacity to enhance cancer therapy by promoting the accumulation of nanomedicine in tumor tissue via selectively augmenting the EPR effect of nanoparticles. The micelle with a negatively charged surface has a long blood circulation time, with a large DOX elimination half-life ($t_{1/2\beta}$ = 12.20 h). Once the micelle arrives in the mildly acidic tumor tissue, the pH-sensitive mPEG layer is shed, exposing both the chelated copper ions and the cRGD peptides. The cRGD peptide allows the micelles to selectively accumulate on tumor blood vessels; the copper ions catalyze the decomposition of the endogenous NO donors (RSNO) in situ to produce NO, dilating tumor blood vessels, and, in turn, causing an increase in vascular permeability. The augmented EPR effect can significantly enhance the accumulation of the micelles in tumor tissue, with a high cumulative content of DOX 48 h after injection. Inside the tumor cells, a rapid intracellular DOX release is achieved by disintegration of the micelles in response to the high levels of cytoplasmic GSH, resulting in an enhanced chemotherapy with a high IR (≈94%) of tumor growth and an excellent survival rate (100%) of the mice. Therefore, this work opens up a new strategy in the development of multifunctional nanocarriers for the fight against malignant tumors.

4. Experimental Section

Materials: Protoporphyrin IX (PpIX) and GSNO were purchased from Aldrich Chemical Co. Ltd. c(RGDfK) was custom-made by Apeptide Co. Ltd. (Shanghai, China). Monomethoxy poly(ethylene glycol) ($mPEG_{2k}$-OH) and OH-PEG_{2K}-OH with molecular weight of 2000 were purchased from Alfa Aesar Chemical Co. Ltd. Doxorubicin hydrochloride

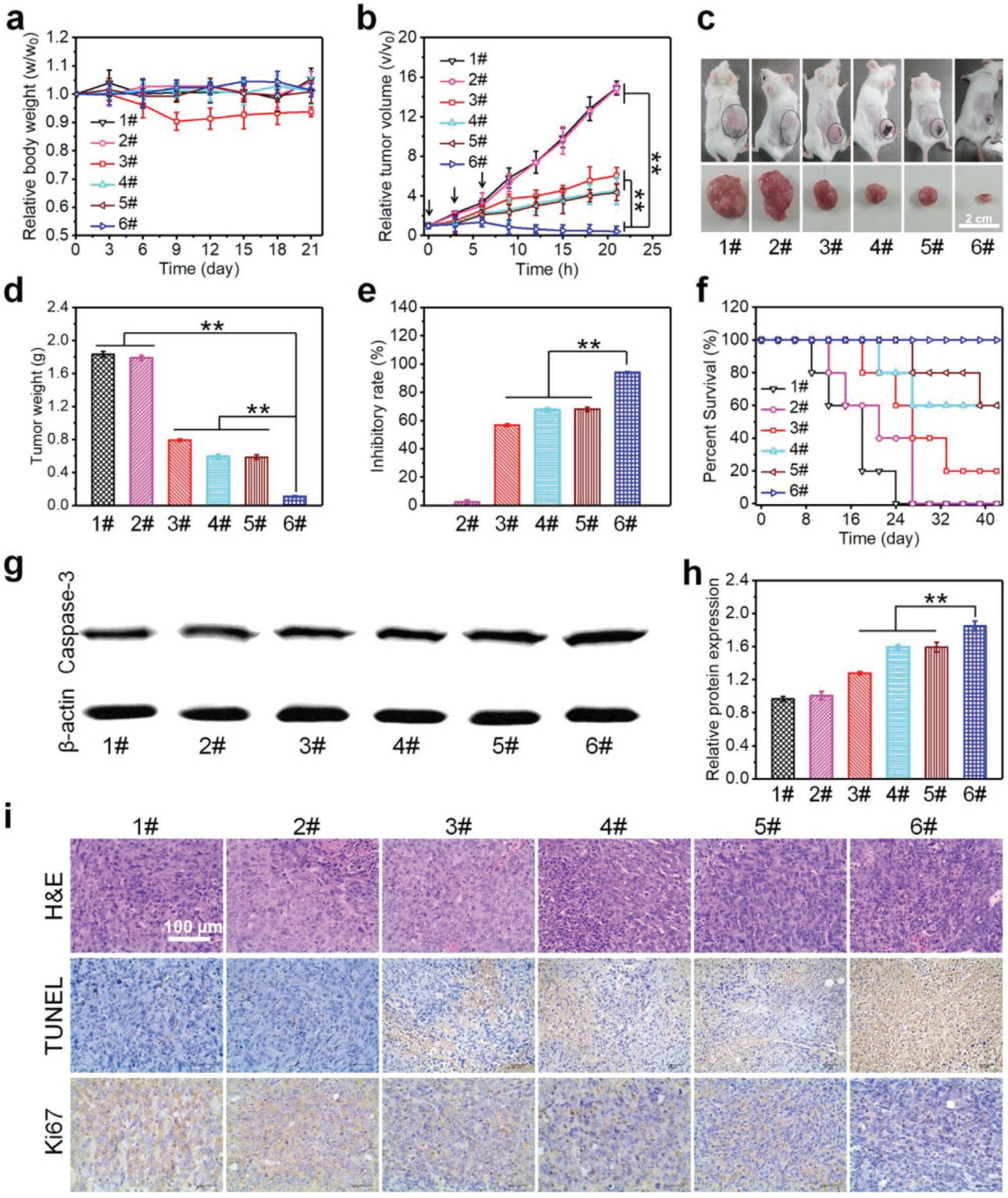

Figure 5. In vivo antitumor activity evaluation. a) Body weight changes of 4T1 tumor-bearing mice after treated with different DOX formulations. b) Tumor volume changes. The black arrows indicate the time points for administration. c) Photographs of the tumor-bearing mice and the excised tumors. d) Tumor weight, e) IR of tumor growth in 16 d treatment. f) Survival curves of the mice after treated with different formulations. g) Representative protein expression determined by Western blot. h) Quantitative analysis of light intensities of relative protein expression from Western blot results. i) Ex vivo histological analyses of tumor sections stained with H&E, TUNEL, and Ki67 at day 16 post-i.v. injection. 1#: Saline. 2#: Cu-PLEPMPss-cRGD hybrid micelles. 3#: Free DOX. 4#: DOX@PLEPMPss-cRGD hybrid micelles. 5#: DOX@Cu-PLEPMPss micelles. 6#: DOX@ Cu-PLEPMPss-cRGD hybrid micelles. The values were expressed as mean ± SD. $^{**}p < 0.01$.

(DOX·HCl) was purchased from Zhejiang Hisun Pharmaceutical Co., Ltd. (China) and DOX was obtained by dehydrochlorination. Dicyclohexylcarbodiimide (DCC), trifluoroacetic acid (TFA), and GSH were purchased from Adamas-beta. 1-Ethyl-3-(3-dimethyllaminopropyl) carbodiimide hydrochloride (EDC·HCl) and *N*-hydroxysuccinimide (NHS) were purchased from Sigma chemicals (St. Louis, MO, USA). Tert-butyl 2-(2-(2-amimoethyl) disulfanyl) ethylcarbamate (Boc-NH-SS-NH_2) and N-Boc-ethylenediamine (Boc-NH-NH_2) were synthesized as our previous report.[56] All the other chemicals were purchased from commercial supplier and used as received.

Cell Lines and Culture Conditions: The mouse breast carcinoma 4T1 and HUVECs were obtained from Sichuan University (China). 4T1 Cells were cultured in RPMI 1640, while HUVEC cells were cultured in F12 medium, both supplemented with 10% (v/v) FBS at 37 °C in a 5% CO_2 atmosphere under fully humidified conditions.

Animals: Female BALB/c mice (18 ± 2 g) were kept at the condition of 25 °C and 55% of humidity and approved by the Institutional Animal Care and Use Committee of Sichuan University. All animal experiments were carried out in compliance with guidelines.

Synthesis of PLA-SS-PEG-PpIX (PLEPss): The PLA-SS-PEG-PpIX (PLEPss) polymer was synthesized by several steps as shown in Scheme 2. First, carboxy-terminated poly(ethylene glycol) (COOH-PEG_{2k}-COOH) was synthesized as previous report.[60] ^{1}H NMR (400 MHz, deuterated chloroform ($CDCl_3$) ; Figure S2, Supporting Information): δ 4.14 (br, −OC***H***$_2$COOH−), 3.63–3.69 (m, −O***CH***$_2$***CH***$_2$O−).

Second, D, L-lactide (6.50 g, 45 mmol) and Boc-NH-SS-NH_2 (0.35 g, 1.3 mmol), were reacted at 140 °C for 4 h through ring-opening polymerization (ROP) with 0.1 wt% $SnCl_2$ as catalyst.[61] After that, the reaction flask was cooled down and dissolved in dichloromethane (DCM), precipitated in cold ethanol, and dried under vacuum to obtain PLA-SS-NH-Boc (yield: 89%). ^{1}H ^{1}H-NMR (400 MHz, $CDCl_3$; Figure S4, Supporting Information): δ 5.16 (m, −C(O)C***H***(CH$_3$)O−), 2.22 (m, −C***H***$_2$NHC(O)−), 2.00 (m, −CH$_2$C***H***$_2$SS−), 1.58 (m, −C(O)CH(C***H***$_3$)O−), 1.26 (s, −C(C***H***$_3$)$_3$).

Third, PLA-SS-NH-Boc (2.0 g, 0.5 mmol) was dissolved in tetrahydrofuran (THF) with TFA (100 µL) and was kept stirring at room temperature (RT) until the Boc was reacted completely under the monitoring with TLC. After that, the reaction solution was concentrated under reduced pressure and then dissolved in DCM, then the COOH-PEG_{2k}-COOH (1.3 g, 0.6 mmol), DCC (0.14 g, 0.68 mmol), and DMAP (0.83 g, 0.68 mmol) were added in the PLA-SS-NH_2 solution above, and kept stirring at RT for at least 48 h. Later, the reaction was quenched by deionized water, and the reaction mixture was filtered and the filtrate was concentrated under vacuum, then the concentrated solution was precipitated into ethanol and dried under vacuum to get PLA-SS-PEG_{2k}-COOH (yield: 75.0%). ^{1}H-NMR (400 MHz, $CDCl_3$) (Figure S5, Supporting Information): δ 5.15 (m, −C(O)C***H***(CH$_3$)O−), 4.20 (m, COOH−C***H***$_2$O−), 4.13 (m, −C(O)C***H***(CH$_3$)OH), 4.03 (m, −OC***H***(CH$_3$)O−), 3.63–3.69 (m, −OC***H***$_2$C***H***$_2$O−), 3.40 (m, −C***H***$_2$NHC(O)−), 2.76 (m, −CH$_2$C***H***$_2$SS−), 1.66 (m, −C(O)CH(C***H***$_3$)O−), 1.26 (m, −C(O)CH(C***H***$_3$)OH).

Fourthly, PpIX (0.2 g, 0.36 mmol), NHS (0.10 g, 0.86 mmol), and DCC (0.18 g, 0.86 mmol) were dissolved in dry THF and stirred at RT in the dark for 0.6 h. Next, the ethylenediamine (266 µL, 4.0 mmol) was added in mixed solution including PpIX, and the mixture was stirred at RT for at least 48 h in the dark. Later, the reaction was quenched by deionized water, and the reaction mixture was filtered and the filtrate was concentrated under vacuum, and the solid material was washed with chilled distilled water and lyophilized to obtain PpIX-NH_2 (yield: 90.3%). FTIR (neat, cm^{-1}) (Figure S6, Supporting Information): 1641, 1552.

Finally, PLA-SS-PEG_{2k}-COOH (1.0 g, 0.16 mmol), NHS (0.02 g, 0.17 mmol), and EDC·HCl (0.04 g, 0.17 mmol) were dissolved in DMF, and the mixture was stirred for 3 h. The PpIX-NH_2 (0.103 g, 0.16 mmol) was dissolved in DMF and dropwise added in above reaction solution, and the mixture was stirred at RT in the dark for 48 h. Later, the reaction mixture was dialyzed (MWCO 1000) against deionized water to remove DMF and unreacted PpIX-NH_2. The PLEPss was collected by lyophilization (yield: 70.3%). ^{1}H-NMR (400 MHz, DMSO-d_6; Figure S7, Supporting Information): δ 6.21–6.48 (m, CH$_2$=C***H***− and −C***H***=C−), 5.22 (m, −C(O)C***H***(CH$_3$)O−), 3.50–3.73 (m, −OC***H***$_2$C***H***$_2$O−), 1.46 (m, −C(O)CH(C***H***$_3$)O−).

Synthesis of PLA-SS-PEG-PpIX-Cu (Cu-PLEPss): The PLEPss polymer with a chelated bivalent copper ion (Cu-PLEPss) was synthesized by the following steps. Excess free bivalent copper ions were first incubated with PLEPss (0.5 g, 0.07 mmol) in DMF for 6 h under nitrogen according to previous method.[52] Later, the free copper ions and DMF were removed by dialyzed (MWCO 3500). Cu-PLEPss was collected by lyophilization (yield: 98.3%).

Synthesis of PLA-SS-PEG-PpIX-Cu-CDM-PEG (Cu-PLEPMPss): First, mPEG_{2k}-CDM was synthesized according to previous method.[49] ^{1}H-NMR (400 MHz, $CDCl_3$; Figure S8, Supporting Information): δ 4.30 (m, −CH$_2$C***H***$_2$O−), 3.62–3.72 (m, −OC***H***$_2$C***H***$_2$O−), 3.36 (s, C***H***$_3$O−), 2.70 (m, −C(O)C***H***$_2$C***H***$_2$−), 2.10 (s, C***H***$_3$−).

Second, the cyclic anhydride of mPEG_{2k}-CDM was opened by an amino group of Cu-PLEPss. In brief, the Cu-PLEPss (0.3 g, 0.04 mmol) was incubated with mPEG_{2k}-CDM (0.18 g, 0.08 mmol) in anhydrous DCM, then the mixture reaction was kept stirring at RT for 48 h. Next, the mixture reaction was dialyzed (MWCO 3500) against deionized water for 3 d to remove unreacted mPEG_{2k}-CDM. Cu-PLEPMPss was collected by lyophilization (yield: 83.0%). ^{1}H-NMR (400 MHz, $CDCl_3$; Figure S9, Supporting Information): δ 6.20–6.51 (m, CH$_2$=C***H***− and −C***H***=C−), 5.21 (m, −C(O)C***H***(CH$_3$)O−), 3.50–3.73 (m, −OC***H***$_2$C***H***$_2$O−), 3.34 (s, C***H***$_3$O−), 1.99 (s, C***H***$_3$−), 1.47 (m, −C(O)CH(C***H***$_3$)O−).

Synthesis of the cRGD Decorated PCL-PEG-cRGD (PCE-cRGD) Polymer: The PCE-cRGD polymer was synthesized by the following three steps as Figure S1 in the Supporting Information. First, the hydrophobic block, polycaprolactone (Boc-NH_2-PCL), was synthesized through ROP of ε-CL initiated by N-Boc-ethylenediamine in the presence of $SnCl_2$ as catalyst.[62] ^{1}H-NMR (400 MHz, $CDCl_3$; Figure S11, Supporting Information): δ 4.06 (t, J = 8.0 Hz, −C***H***$_2$OC(O)−), 3.87 (t, J = 4.0 Hz, −C***H***$_2$OH), 3.72 (m, −C(O)NHC***H***$_2$C***H***$_2$NHC(O)−), 2.31 (t, J = 8.0 Hz, −C(O)C***H***$_2$−), 1.65 (m, −C(O)C***H***$_2$C***H***$_2$CH$_2$C***H***$_2$−), 1.38 (m, −C(O)(CH$_2$)$_2$C***H***$_2$CH$_2$−), 1.18 (s, −C(C***H***$_3$)$_3$).

Second, the amphiphilic copolymer, PCL-PEG_{2k}-COOH, was synthesized by a condensation reaction between the amino and carboxyl groups. ^{1}H-NMR (400 MHz, $CDCl_3$; Figure S12, Supporting Information): δ 4.14 (s, −C(O)CH_2O−), 4.09 (t, J = 8.0 Hz, −C***H***$_2$OC(O)−), 3.64 (m, −OC***H***$_2$C***H***$_2$O−), 3.46 (t, J = 4.0 Hz, −C***H***$_2$OH), 3.12 (−NHC***H***$_2$C***H***$_2$NH−), 2.30 (t, J = 8.0 Hz, −C(O)C***H***$_2$−), 1.63 (m, −C(O)CH$_2$C***H***$_2$C***H***$_2$CH$_2$−), 1.37 (m, −C(O)(CH$_2$)$_2$C***H***$_2$CH$_2$−).

Finally, *N*-(2-(t-Boc)-aminoethyl) maleimide (DDC) was synthesized, and took off the Boc and grafted to the end of the PCL-PEG_{2k}-COOH block.[63] After that, cRGD was grafted to the DDC using "click chemistry." ^{1}H-NMR (400 MHz, DMSO-d_6; Figure S14, Supporting Information): δ 7.25–6.90 (m, Ph), 4.63–4.44 (m, −NHC***H***(CH$_2$)C(O)−), 4.14 (m, −CHC***H***$_2$C(O)−, −CH$_2$C***H***C(S)C(O)− and −C***H***$_2$C***H***$_2$NH−), 3.96 (brs, −C***H***$_2$OC(O)−), 3.51 (m, −O***CH***$_2$***C***H$_2$O−), 2.26 (brs, −C(O)C***H***$_2$−), 1.55 (m, −C(O)CH$_2$C***H***$_2$***C***H$_2$CH$_2$−), 1.30 (m, −C(O)(CH$_2$)$_2$C***H***$_2$CH$_2$−).

Characterization of Polymers: The chemical structure of synthesized polymers were confirmed by ^{1}H NMR spectra, which were recorded at RT on a Bruker AM 300 apparatus. $CDCl_3$ and dimethyl sulfoxide DMSO-d_6 were used as a solvent, and tetra-methylsilane was used as the internal reference. FT-IR spectra were obtained with a Nicolet 5700 spectrometer in the range of 4000–500 cm^{-1}. KBr tablets were prepared by grinding the polymers with KBr and compressing the powders into a transparent tablet.

Preparation of Blank Hybrid Micelles and DOX-Loaded Hybrid Micelles: A solvent evaporation method was applied to prepare blank hybrid micelles and DOX-loaded hybrid micelles. For instance, to prepare the blank hybrid micelles or DOX-loaded hybrid micelles with the Cu-PLEPss/PCE-cRGD weight ratio of 8:2, the followed steps were taken. First, 8 mg of Cu-PLEPMPss polymer and 2 mg of PCE-cRGD polymer with or without 1 mg DOX·HCl were dissolved in 10 mL THF. A drop of TEA was added if DOX·HCl was present. The solution was then added dropwise into 10 mL deionized water under high-speed stirring.

Subsequently, the blank hybrid micelles (Cu-PLEPMPss-cRGD hybrid micelles) or DOX-loaded hybrid micelles (DOX@Cu-PLEPMPss-cRGD) gradually formed with the evaporation of THF. Afterward, the DOX-loaded hybrid micellar solutions were dialyzed (MWCO 1000) against deionized water for 3 d to completely remove the unloaded drug. Finally, the DOX-loaded hybrid micelles were collected by lyophilization.

Characterization of Micelles: Pyrene (Aladdin Industrial Corporation) was chosen as a fluorescence probe to determine the CMC of Cu-PLEPMPss micelles, PCE-cRGD and Cu-PLEPMPss-cRGD hybrid micelles.[64] The pyrene excitation spectra were recorded on a Hitach F-7000 spectra fluorophotometer. The micelle size and zeta potential were measured at 25 °C by DLS (Zeta-Sizer, Malvern Nano-ZS90, Malvern, U.K.). The morphologies of micelles were observed by TEM, which was performed with a JEOL 2010F instrument (JEOL Ltd., Japan). The UV–vis spectrum of PpIX and the polymers which were grated PpIX or chelated bivalent copper ion were acquired, and DLC and EE of the DOX-loaded micelles were determined by a UV–VIS spectrophotometer (UV-2550, Shimadzu, Japan). The concentration of copper ions was measured by ICP-MS (Xseries II, Thermoscientific, USA) or ICP-OES (Avio 200, Platinum Elmer, USA).

Optimization of the Ratio of Cu-PLEPss and PCE-cRGD Components in Hybrid Micelles: The optimal ratio of Cu-PLEPss and PCE-cRGD components in hybrid micelles was confirmed by flow cytometer (FCM). In brief, 10×10^4 cells per well of HUEC cells were seeded in 6-well plate with F12 medium and incubated for 24 h at 37 °C. Then different ratios of DOX-loaded hybrid micelles were added to each well (DOX-equivalent dose: 5 μg mL^{-1}) for further 1 h incubation. The drug-free culture medium was applied as a blank control. After that, the cells were washed with PBS for three times, harvested by trypsinization, centrifuged (1500 rpm, 5 min), and re-suspended in PBS. The DOX fluorescence intensity was measured by a FCM (BD Biosciences, USA). To verify the optimal ratio of micelles, the 4T1 cells were used and the operation process was same as above. To investigate the cRGD-receptor mediated internalization of DOX-loaded hybrid micelles, 1 mg L^{-1} of free cRGD was incubated with 4T1 cells for 2 h before the addition of DOX@Cu-PLEPss-cRGD hybrid micelles.

In Vitro Catalytic Generation of NO: The NO generation catalyzed by various blank micelles was tested by a chemiluminescence NOA (Seivers 280i, Boulder, CO), Griess method and fluorescent indicator of NO, respectively. For the chemiluminescence analysis, 5 mL of the PBS containing 10 μmol RSNO and 10 μmol GSH was transported to the NOA by a stream of N_2 (g), and the various blank micelles were added into after testing baseline became smooth. Next, the amount of NO generated was calculated according to the calibration curves of the NOA. For the Griess kit analysis, a 48-well plate was covered by 1 mL of the PBS solution or F12 medium (10% FBS), which containing 10 μmol GSNO and 10 μmol GSH, then different concentrations or different kinds of blank micelles were added and incubated. Afterward, 200 μL of solution was removed at the predetermined time for Griess reagents detection according to the directions. Nitrite concentrations were calculated with reference to a standard curve of sodium nitrite generated by known concentrations. For fluorescence detection analysis, HUVEC cells were seeded into 6-well plate a density of 10×10^4 cells per well or 48-well plate at a density of 1×10^4 cells per well with F12 medium containing 10% FBS with 10×10^{-6} M GSNO 10×10^{-6} M GSH at 37 °C with 5% CO_2 for 24 h. After that, the medium was removed and replaced with fresh medium, then the cells were treated with different concentrations or different kinds of blank micelles at pH 7.4 or 6.5, and incubated for predetermined time. After treatment, the cells were washed twice with PBS. The blank control groups with cells only incubated without any micelles for corresponding times. For the detection purpose, the cells were fixed with PBS containing the 5×10^{-6} M DAF-FM DA and incubated at 37 °C for 30 min, then the cells washed by PBS solution three times to remove excess probe and covered with PBS. The cells were subjected to observation using a fluorescence microscope (Olympus, CKX41) or CLSM (Leica TCS SP8, Leica, Germany). The NO fluorescence intensity of the cells were read by an automated microplate spectrophotometer (ELX800 Biotek, USA) at an excitation wavelength of 495 nm and an emission wavelength of 515 nm. The NO fluorescence intensity was also measured by FCM (BD Biosciences, USA) at a same excitation wavelength and emission wavelength above.

Determination of Reduction and pH Sensitivity of Micelles: To determine the reduction sensitivity, DLS was performed to measure the average size of the Cu-PLEPMPss-cRGD hybrid micelles in PBS (pH 7.4 and 6.5) or ABS (pH 5.0) with different GHS concentrations (10 μmol and 10 mmol). To determine the pH sensitivity, DLS was performed to measure the average size and zeta potential of the Cu-PLEPMPss-cRGD hybrid micelles in PBS at pH 7.4 or 6.5. ^{1}H NMR was also used to determine the pH sensitivity of Cu-PLEPMPss-cRGD hybrid micelles. After the micelles was incubated in PBS at pH 6.5 or 7.4 for predetermined time intervals, the solution was collected and freeze-dried for the characterization of ^{1}H NMR.

In Vitro DOX release: The preweighed DOX@Cu-PLEPMPss-cRGD powders were dispersed in PBS at pH 7.4 or 6.5 containing 10×10^{-6} M or 10×10^{-3} M GSH or ABS at pH 5.0 containing 10×10^{-6} M or 10×10^{-3} M GSH, and dialyzed against the relevant dispersion medium at 37 °C in the dark. Then 1 mL of external buffer was removed at the predetermined time and replaced with 1 mL of fresh medium. The amount of released DOX was detected by a Fluoromax spectrometer.

Cellular Uptake and Intracellular Accumulation: CLSM was used to evaluate the in vitro cellular uptake behaviors and intracellular accumulation of free DOX and DOX-loaded micelles in 4T1 cells. 4T1 cells were seeded in 6-well at a density of 10×10^4 cells per well with RPMI 1640 medium. After 24 h of incubation at 37 °C, the cells were treated with free DOX, DOX@Cu-PLEPMPss micelles, and DOX@Cu-PLEPMPss-cRGD hybrid micelles (DOX-equivalent dose: 5 μg mL^{-1}) for 1 and 6 h. Later, the cells were washed twice with PBS, fixed with 2.5% glutaraldehyde for 20 min. The nucleus were stained with 4′, 6-diamidino-2-phenylindole (DAPI) for 8 min. CLSM images were obtained using a Leica Microsystems CMS Gmbh (TCS SP5, Germany). The excitation and emission wavelength of DAPI was 340 and 488 nm, respectively. The excitation and emission wavelength of DOX was 485 and 595 nm, respectively.

In Vitro Cell Cytotoxicity Assay: The cytocompatibility of blank micelles were evaluated by AB assay and live/dead staining. For the AB assay, HUVEC and 4T1 cells were seeded in 48-well plates with RPMI 1640 medium (pH 6.5) at a density of 1×10^4 cells per well. After 24 h of incubation at 37 °C, the blank Cu-PLEPMPss-cRGD hybrid micelles with different concentrations ranging from 10 to 250 μg mL^{-1} were added to each well respectively, and cultured for an additional 24 h. Afterward, the culture medium was removed and the cells were washed with PBS (pH 7.4) for three times, and then 300 μL AB solution (10% AB, 80% media 199 (Gibcos) and 10% FBS, v/v) was added and for further 3 h incubation. 200 μL of AB solution was then transferred into a 96-well plate from the 48-well plates. The absorbances of the solution were read by an automated microplate spectrophotometer (ELX800 Biotek, USA) at 570 nm. For live/dead staining, 2×10^4 cells per well of HUVEC and 4T1 cells were seeded in 24-well plates, and the cells were stained by calceinacetoxy methylester (Calcein-AM, 2×10^{-3} M) for 15 min after 24 h incubation with different concentrations of blank Cu-PLEPMPss-cRGD hybrid micelles. Live cells were stained green by fluorescence microscope (Olympus, CKX41). The cytotoxicity study of DOX@Cu-PLEPMPss micelles and DOX@Cu-PLEPMPss-cRGD hybrid micelles with 4T1 cells were also evaluated through the similar method as described above.

In order to investigate whether the catalytic production of NO at the concentration influence the growth of the 4T1 tumor cells, 4T1 cells were seeded in 6-well or 48-well plates with RPMI 1640 medium. After 24 h of incubation at 37 °C, the medium was removed and replaced with fresh medium containing 10% FBS, 10×10^{-6} M GSNO, and 10×10^{-6} M GSH, then the cells was treated with Cu-PLEPss-cRGD hybrid micelles at a copper ion concentration of 0.7 μg mL^{-1}, and cultured for an additional 6, 12, or 24 h. Afterward, the culture medium was removed and the cells were washed with PBS for three times, then the cell viability was detected via live/dead staining and AB assay, respectively.

In Vivo and Ex Vivo DOX Fluorescence Imaging: Free DOX, DOX@Cu-PLEPMPss micelles, and DOX@Cu-PLEPMPss-cRGD hybrid micelles

were, respectively, injected into 4T1 tumor-bearing nude mice via lateral tail vein at a dosage of 2 mg DOX/kg body weight. 0.9% NaCl solution was used as control. The mice were then anesthetized and imaged by Maestro In-Vivo Imaging System at prescribed time points (1, 3, and 6 h). After 6 h injection, the mice were sacrificed and the normal organs (heart, liver, spleen, lung, and kidney) as well as tumors were excised for ex vivo imaging to observe the distribution of DOX fluorescence. The emission fluorescence was collected from 500 to 750 nm, and the 455 nm excitation filter was used.

In Vivo Evaluation of Blood Circulation and Biodistribution: Female BALB/C mice were intravenously injected with free DOX and DOX@PLEPMPss-cRGD, DOX@Cu-PLEPMPss, and DOX@Cu-PLEPMPss-cRGD solutions corresponding to 2 mg kg^{-1} DOX body weight. Blood samples were obtained via eyeball extirpating at prescribed time points (1, 3, 6, 12, and 24 h) postinjection using a heparinized capillary tube, and then centrifuged at 3000 rpm min^{-1} for 10 min. The plasma was collected and tested by fluorescence spectra. In order to test the tissue distribution, mice bearing 4T1 tumor were injected with free DOX, DOX@PLEPMPss-cRGD, DOX@Cu-PLEPMPss, and DOX@Cu-PLEPMPss-cRGD solutions with the same dose of DOX and sacrificed at the same time points postinjection. Major organs (heart, liver, spleen, lung, kidney, and tumor) were collected, weighed, and homogenized in 2 mL DMSO, respectively. Then, the DMSO solutions were centrifuged for 10 min at 3500 rpm min^{-1}, and the supernatants were collected and measured using a Fluoromax spectrometer. The biodistribution of Cu-PLEPMPss and Cu-PLEPMPss-cRGD at 6 and 24 h after i.v. injection into 4T1 tumor-bearing mice was determined by copper ion radioactivity measurement in various organs and tissues via the ICP-OES analysis. The percent of the injected dose of the DOX or copper ion reached the tissue (%ID) and the percent ID per gram of tissue (%ID/g) values were calculated using the following equations.

$$\%\mathrm{ID} = \frac{\text{dose in blood/tissue sample}}{\text{injected dose}} \times 100 \quad (1)$$

$$\%\mathrm{ID/g} = \frac{\mathrm{ID}\%}{\text{weight of tissue(g)}} \quad (2)$$

In Vivo Antitumor Study: 4T1 tumor-bearing mice were randomly divided into six groups (six mice per group). 0.9% NaCl, Cu-PLEPMPss-cRGD blank hybrid micelles and free DOX or DOX@PLEPMPss-cRGD, DOX@Cu-PLEPMPss, and DOX@Cu-PLEPMPss-cRGD were intravenously injected into mice every 3 d for three times at a dosage of 2 mg DOX kg^{-1} body weight. The tumor sizes and mice body weight were measured every 3 d, and the volume was calculated according to the formula: $V = 0.5 \times a \times b^2$, where in a is the length of the tumor and b is the width of the tumor. The mice survival was recorded.

Frozen Section Preparation: 4T1 tumor-bearing mice were treated with free DOX or DOX@PLEPMPss-cRGD, DOX@Cu-PLEPMPss and DOX@Cu-PLEPMPss-cRGD solutions at a dosage of 2 mg DOX kg^{-1} body weight. A solution of 0.9% NaCl was used as control. The tumors were isolated at prescribed time points (6 and 24 h) postinjection, embedded in optimal cutting temperature compound and cut into 6 µm slices. For CD31 staining, rat-anti-mouse CD31 antibody was used as the primary antibody, while donkey-anti-rat antibody conjugated with rhodamine was used as the secondary antibody. After staining, all sections were stained with DAPI and observed by fluorescence microscope or CLSM.

Western Blotting Analysis: For the Western blotting analysis, the tumors were lysed on ice by RIPA buffer (RIPA:Cocktail = 100:1) and centrifuged at 12 000 rpm min^{-1} for 10 min to collect the supernatant. The total protein was quantified by the BCA protein assay kit (KGPBCA, KeyGEN). A sample of 100 µg of protein was electrophoresed in 10% SDS-PAGE and transferred to a nitro-cellulose membrane, blocked and incubated overnight with rabbit monoclonal anti-caspase-3 antibody (ABCAM). After washing thrice with TBST buffer every 5 min, the membrane was incubated with horseradish peroxidase conjugated secondary antibody HRP-labeled goat anti-rabbit IgG (ABCAM) for 2–3 h and then rinsed thrice with TBST buffer every 10 min. Rabbit monoclonal anti-β-actin antibody (Santa Cruz Biotechnology) was used as protein loading control. The target protein bands were visualized using the ECL kit (Thermo Scientific).

Systemic Toxicity In Vivo: For the histological analysis, 4T1 tumor-bearing mice were sacrificed at day 16 after the first treatment, and the normal organs (heart, liver, spleen, lung, and kidney) as well as tumors were collected and fixed in 10% formalin and embedded in paraffin blocks to prepare tumor sections at a thickness of 5 µm. After deparaffinization, the tissue sections were stained with H&E, terminal deoxynucleotidyltransferase mediated UTP end labeling (TUNEL) and Ki-67 (Abcam, Cambridge) and were visualized by an optical microscope (Olympus, Japan). For serum analysis, the blood of mice was extracted from Cu-PLEPMPss-cRGD hybrid micelles and saline mice groups at the 16th day (the dosage and frequency were consistent with the antitumor study in vivo). The blood samples were solidified and centrifuged at 3000 rpm for 5 min to obtain serum. The blood biochemistry and hematology analysis of the serum samples were detected at Chengdu Lilai Biotechnology CO. TLD. (Chengdu, China) and data were mean of three replicates.

Statistical Analysis: All experiments data were from at least three independent measurements ($n \geq 3$), and the data were expressed as means ± SD. To determine statistical significance of the data, the single factorial analysis of variance was performed. Statistically significant values were presented as $^{**}p < 0.01$.

Supporting Information

Supporting Information is available from the Wiley Online Library or from the author.

Acknowledgements

This work was partially supported by the China National Funds for Distinguished Young Scientists (51725303), the National Natural Science Foundation of China (21574105, 81701831, 51703189), the Sichuan Province Youth Science and Technology Innovation Team (2016TD0026), and Doctoral Innovation Fund Program of Southwest Jiaotong University (2017).

Conflict of Interest

The authors declare no conflict of interest.

Keywords

drug delivery, EPR effects, nanoparticles, nitric oxide, vasodilation

Received: August 31, 2018
Revised: November 7, 2018
Published online:

[1] Y. Matsumura, H. Maeda, *Cancer Res.* **1986**, *46*, 6387.
[2] H. Maeda, K. Tsukigawa, J. Fang, *Microcirculation* **2016**, *23*, 173.
[3] S. Taurin, H. Nehoff, K. Greish, S. Taurin, H. Nehoff, K. Greish, *J. Controlled Release* **2012**, *164*, 265.
[4] F. Li, J. Lu, X. Kong, T. Hyeon, D. Ling, *Adv. Mater.* **2017**, *29*, 1605897.
[5] C. Zhang, D. Ni, Y. Liu, H. Yao, W. B. Bu, J. Shi, *Nat. Nanotechnol.* **2017**, *12*, 378.

[6] A. K. Iyer, G. Khaled, J. Fang, H. Maeda, *Drug Discovery Today* **2006**, *11*, 812.
[7] J. Fang, H. Nakamura, H. Maeda, *Adv. Drug Delivery Rev.* **2011**, *63*, 136.
[8] J. W. Nichols, Y. H. Bae, *J. Controlled Release* **2014**, *190*, 451.
[9] H. Maeda, *Adv. Drug Delivery Rev.* **2015**, *91*, 3.
[10] L. E. Gerlowski, R. K. Jain, *Microvasc. Res.* **1986**, *31*, 288.
[11] Y. H. Bae, K. Park, *J. Controlled Release* **2011**, *153*, 198.
[12] E. A. Sykes, Q. Dai, C. D. Sarsons, J. Chen, J. V. Rocheleau, D. M. Hwang, G. Zheng, D. T. Cramb, K. D. Rinker, W. C. W. Chan, *Proc. Natl. Acad. Sci. U. S. A.* **2016**, *113*, E1142.
[13] S. Wilhelm, A. J. Tavares, Q. Dai, S. Ohta, J. Audet, H. F. Dvorak, W. C. W. Chan, *Nat. Rev. Mater.* **2016**, *1*, 16014.
[14] S. Ohta, D. Glancy, W. C. W. Chan, *Science* **2016**, *351*, 841.
[15] S. Huang, S. Duan, J. Wang, S. Bao, X. Qiu, C. Li, Y. Liu, L. Yan, Z. Zhang, Y. Hu, *Adv. Funct. Mater.* **2016**, *26*, 2532.
[16] D. P. Lankveld, R. G. Rayavarapu, P. Krystek, A. G. Oomen, H. W. Verharen, T. G. van Leeuwen, W. H. De Jong, S. Manohar, *Nanomedicine* **2011**, *6*, 339.
[17] E. Gullotti, Y. Yeo, *Mol. Pharmaceutics* **2009**, *6*, 1041.
[18] Y. Zhang, P. Li, H. Pan, L. Liu, M. Ji, N. Sheng, C. Wang, L. Cai, Y. Ma, *Biomaterials* **2016**, *83*, 219.
[19] Y. Wang, G. Wei, X. Zhang, F. Xu, X. Xiong, S. Zhou, *Adv. Mater.* **2017**, *29*, 1605357.
[20] T. P. Thomas, B. H. Huang, S. Ki Choi, J. E. Silpe, A. Kotlyar, A. M. Desai, H. Zong, J. Gam, M. Joice, J. R. Baker, *Mol. Pharmaceutics* **2012**, *9*, 2669.
[21] L. Li, L. Song, X. Liu, X. Yang, X. Li, T. He, N. Wang, S. Yang, C. Yu, T. Yin, Y. Wen, Z. He, X. Wei, W. Su, Q. Wu, S. Yao, C. Gong, Y. Wei, *ACS Nano* **2017**, *11*, 95.
[22] Z. Ge, Q. Chen, K. Osada, X. Liu, T. A. Tockary, S. Uchida, A. Dirisala, T. Ishii, T. Nomoto, K. Toh, Y. Matsumoto, M. Oba, M. R. Kano, K. Itaka, K. Kataoka, *Biomaterials* **2014**, *35*, 3416.
[23] S. H. Crayton, A. Tsourkas, *ACS Nano* **2011**, *5*, 9592.
[24] S. Han, Z. Li, J. Zhu, K. Han, Z. Zeng, W. Hong, W. Li, H. Jia, Y. Liu, R. Zhuo, X. Zhang, *Small* **2015**, *11*, 2543.
[25] T. Mizuhara, K. Saha, D. F. Moyano, C. S. Kim, B. Yan, Y. K. Kim, V. M. Rotello, *Angew. Chem., Int. Ed.* **2015**, *54*, 6567.
[26] L. M. R. Ferreira, *Exp. Mol. Pathol.* **2010**, *89*, 372.
[27] P. Huang, Y. Gao, J. Lin, H. Hu, Hsien-S. Liao, X. Yan, Y. Tang, A. Jin, J. Song, G. Niu, G. Zhang, F. Horkay, X. Chen, *ACS Nano* **2015**, *9*, 9517.
[28] H. Li, J. Du, X. Du, C. Xu, C. Sun, H. Wang, Z. Cao, X. Yang, Y. Zhu, S. Nie, J. Wang, *Proc. Natl. Acad. Sci. U. S. A.* **2016**, *113*, 4164.
[29] K. Han, J. Zhang, W. Zhang, S. Wang, L. Xu, C. Zhang, X. Zhang, H. Han, *ACS Nano* **2017**, *11*, 3178.
[30] X. Hu, P. He, G. Qi, Y. Gao, Y. Lin, C. Yang, P. Yang, H. Hao, L. Wang, H. Wang, *ACS Nano* **2017**, *11*, 4086.
[31] M. J. Ernsting, M. Murakami, *J. Controlled Release* **2013**, *172*, 782.
[32] V. P. Chauhan, T. Stylianopoulos, Y. Boucher, R. K. Jain, *Annu. Rev. Chem. Biomol. Eng.* **2011**, *2*, 281.
[33] M. I. Setyawati, V. N. Mochalin, D. T. Leong, *ACS Nano* **2016**, *10*, 1170.
[34] R. F. Furchgott, J. V. Zawadzki, *Nature* **1980**, *288*, 373.
[35] L. J. Ignarro, G. M. Buga, K. S. Wood, R. E. Byrns, G. Chaudhuri, *Proc. Natl. Acad. Sci. U. S. A.* **1987**, *84*, 9265.
[36] R. M. J. Palmer, A. G. Ferrige, S. Moncada, *Nature* **1987**, *327*, 524.
[37] Po-T. Kao, I-J. Lee, I. Liau, C. S. Yeh, *Chem. Sci.* **2017**, *8*, 291.
[38] M. Kelm, *Biochim. Biophys. Acta, Bioenerg.* **1999**, *1411*, 273.
[39] J. Albert, M. Daleskog, N. H. Wallén, *Thromb. Res.* **2001**, *102*, 161.
[40] H. Al-sa'Doni, A. Ferro, *Clin. Sci.* **2000**, *98*, 507.
[41] J. McAninly, D. L. H. Williams, S. C. Askew, A. R. Butlerb, C. Russellb, *J. Chem. Soc., Chem. Commun.* **1993**, *23*, 1758.
[42] P. Wang, M. Xian, X. Tang, X. Wu, Z. Wen, T. Cai, A. J. Janczuk, *Chem. Rev.* **2002**, *102*, 1091.
[43] Y. Ishima, D. Chen, J. Fang, H. Maeda, A. Minomo, U. Kragh-Hansen, T. Kai, T. Maruyama, M. Otagiri, *Bioconjugate Chem.* **2012**, *23*, 264.
[44] D. Lyn, H. Williams, *Acc. Chem. Res.* **1999**, *32*, 869.
[45] B. K. Oh, M. E. Meyerhoff, *J. Am. Chem. Soc.* **2003**, *125*, 9552.
[46] G. Chen, L. Wang, T. Cordie, C. Vokoun, K. W. Eliceiri, S. Q. Gong, *Biomaterials* **2015**, *47*, 41.
[47] D. H. Kim, A. C. Larson, *Biomaterials* **2015**, *56*, 154.
[48] H. Shi, J. Liu, J. Geng, B. Tang, B. Liu, *J. Am. Chem. Soc.* **2012**, *134*, 9569.
[49] C. Sun, Y. Liu, J. Du, Z. Cao, C. Xu, J. Wang, *Angew. Chem., Int. Ed.* **2016**, *55*, 1010.
[50] X. Guo, X. Wei, Y. Jing, S. Zhou, *Adv. Mater.* **2015**, *27*, 6450.
[51] X. Wei, Y. Wang, X. Xiong, X. Guo, L. Zhang, X. Zhang, S. Zhou, *Adv. Funct. Mater.* **2016**, *26*, 8266.
[52] Y. Li, T. Lin, Y. Luo, Q. Liu, W. Xiao, W. Guo, D. Lac, H. Zhang, C. Feng, S. Wachsmann-Hogiu, J. H. Walton, S. R. Cherry, D. J. Rowland, D. Kukis, C. X. Pan, K. S. Lam, *Nat. Commun.* **2014**, *5*, 4712.
[53] S. D. Conner, S. L. Schmid, *Nature* **2003**, *422*, 37.
[54] D. Peer, J. M. Karp, S. Hong, O. C. Farokhzad, R. Margalit, R. Langer, *Nat. Nanotechnol.* **2007**, *2*, 751.
[55] M. Prabaharan, J. J. Grailer, S. Pilla, D. A. Steeber, S. Gong, *Biomaterials* **2009**, *30*, 3009.
[56] Y. Wang, L. Zhang, X. Zhang, X. Wei, Z. Tang, S. Zhou, *ACS Appl. Mater. Interfaces* **2016**, *8*, 5833.
[57] H. Gong, Y. Chao, J. Xiang, X. Han, G. Song, L. Feng, J. Liu, G. Yang, Q. Chen, Z. Liu, *Nano Lett.* **2016**, *16*, 2512.
[58] S. Wang, P. Huang, X. Chen, *Adv. Mater.* **2016**, *28*, 7340.
[59] E. Jabbari, X. Yang, S. Moeinzadeh, X. He, *Eur. J. Pharm. Biopharm.* **2013**, *84*, 49.
[60] S. C. Grindy, R. Learsch, D. Mozhdehi, J. Cheng, D. G. Barrett, Z. Guan, P. B. Messersmith, N. Holten-Andersen, *Nat. Mater.* **2015**, *14*, 1210.
[61] X. Guo, C. Shi, G. Yang, J. Wang, Z. Cai, S. Zhou, *Chem. Mater.* **2014**, *26*, 4405.
[62] X. Guo, C. Shi, J. Wang, S. Di, S. Zhou, *Biomaterials* **2013**, *34*, 4544.
[63] F. Liu, A. S. Y. Ni, Y. J. Lim, H. Mohanram, S. Bhattacharjya, B. G. Xing, *Bioconjugate Chem.* **2012**, *23*, 1639.
[64] S. Zhou, X. Deng, H. Yang, *Biomaterials* **2003**, *24*, 3563.